Research Square

Preprints are preliminary reports that have not undergone peer review.
They should not be considered conclusive, used to inform clinical practice,
or referenced by the media as validated information.

Regularization and Stability-Bifurcation-Chaos Trilogy for Caputo Fractional Replicator Dynamics with Global Lipschitz Guarantees

Tongxing Li

tsultx@126.com

Taishan University

Yongfeng Zhang

Taishan University

Xiaodong Zhao

Taishan University

Jianzhong Zhang

Taishan University

Chengdai Huang

Xinyang Normal University

Article

Keywords: Caputo fractional-order system, Regularized replicator dynamics, Fractional Hopf bifurcation, Chaos criterion, Positive invariance, Benchmark comparison, Behavioral data calibration

Posted Date: August 23rd, 2026

DOI: https://doi.org/10.21203/rs.3.rs-10486604/v1

License: This work is licensed under a Creative Commons Attribution 4.0 International License.
Read Full License

Additional Declarations: No competing interests reported.

Regularization and Stability-Bifurcation-Chaos Trilogy for Caputo Fractional Replicator Dynamics with Global Lipschitz Guarantees

Tongxing Li[1,*], **Yongfeng Zhang**[1], **Xiaodong Zhao**[1], **Jianzhong Zhang**[1], **and Chengdai Huang**[2]

[1]Taishan University, School of Mathematics and Statistics, Tai'an, 271000, China
[2]Xinyang Normal University, School of Mathematics and Statistics, Xinyang 464000, China
[*]tsultx@126.com

ABSTRACT

Classical fractional-order replicator dynamics are inherently ill-posed owing to the $0/0$ indeterminacy of the average payoff at the origin. The present work constructs a regularized three-dimensional Caputo fractional replicator system coupled with emotional game factors, and establishes four principal contributions. First, a singularity-eliminating regularization operator is introduced to circumvent the topological obstruction at the origin, supported by rigorous proofs of global Lipschitz continuity and positive invariance of the feasible domain under suitable boundary dominance conditions. Second, by invoking the fractional comparison lemma and center manifold reduction, the critical fractional-order threshold is derived in closed form, and the supercritical nature of the memory-induced Hopf bifurcation is analytically verified through an explicit algebraic discriminant. Third, within the fractional Oseledets ergodic framework, a multi-condition composite criterion for chaotic signature identification is formulated that integrates the maximum Lyapunov exponent with positive topological entropy, thereby providing a robust framework for chaos certification. Fourth, the complete three-stage dynamical transition, from asymptotic stability through limit-cycle oscillations to deterministic chaos is systematically characterized under the proposed framework. Crucially, the work provides extensive quantitative benchmark simulations against three representative unregularized fractional replicator models from the literature, complemented by real questionnaire-based behavioral data calibration that empirically grounds the theoretical framework. Collectively, these results demonstrate the superior numerical stability and global well-posedness of the proposed regularized framework relative to classical baseline formulations within the parameter regimes investigated.

Keywords: Caputo fractional-order system; Regularized replicator dynamics; Fractional Hopf bifurcation; Chaos criterion; Positive invariance; Benchmark comparison; Behavioral data calibration

1 Introduction

Fractional-order differential equations have gained widespread popularity in evolutionary game dynamics owing to their intrinsic capability to capture memory-dependent evolutionary trajectories that integer-order models cannot reproduce. The fractional replicator equation serves as the core mathematical tool for describing bounded rational decision-making among multi-agent populations, and it has been extensively extended to emotional game systems, social group competition, and intelligent swarm evolution in recent years. Compared with classical integer-order evolutionary dynamics, Caputo fractional derivatives introduce historical state memory kernels, which precisely characterize the cumulative psychological perception and delayed response of game participants during repeated strategy updating. Such modeling advantages render fractional replicator dynamics a fundamental framework for analyzing human behavioral evolution, with promising applications in cultural communication, group public opinion propagation, and intelligent agent collaborative decision-making.

Despite the prosperous development of fractional replicator dynamic modeling, several open challenges persist in the current literature, which motivate the present investigation. First, the mathematical well-posedness of classical formulations near the origin remains an open challenge owing to the $0/0$ indeterminacy in the average payoff. Representative works[3,7,12] circumvent this singularity by restricting simulation domains to regions away from the origin, while a rigorous global regularization framework with Lipschitz guarantees has not been established in the context of fractional replicator dynamics. Existing studies rely primarily on local discrete numerical experiments without providing global analytical validity verification.

Second, systematic stability analysis for boundary equilibria in fractional replicator systems faces technical difficulties. Current approaches typically employ full-dimensional Jacobian matrices for stability discrimination; however, this practice

introduces spurious zero eigenvalues at strategy boundary equilibria, potentially leading to distorted stability conclusions for mixed-strategy populations. A dimension-adaptive linearization strategy that correctly accounts for the reduced dynamics on boundary manifolds remains to be developed.

Third, complete topological criteria for bifurcation and chaos identification in fractional-order evolutionary systems are not yet fully established. Existing Hopf bifurcation analyses have not derived closed-form critical fractional orders for singular replicator equations, and chaos identification has relied predominantly on a single positive fractional Lyapunov exponent. This practice may lead to false-positive identifications for weak chaotic attractors, as it lacks corroborating topological evidence such as positive topological entropy or Poincaré section characteristics. A notable gap in previous studies is the absence of quantitative benchmarking against published models or systematic real experimental calibration, which restricts the reliability and practical applicability of theoretical conclusions.

To address the aforementioned research gaps, this paper proposes a unified regularized three-dimensional Caputo fractional emotional replicator dynamic framework that systematically tackles the three core limitations summarized above. A dedicated singularity elimination regularization operator is embedded into the fractional replicator equation to realize global Lipschitz continuity and circumvent the origin indeterminate singularity. This regularization strategy follows the general philosophy of singular perturbation regularization in fractional differential systems[2,11], while extending its application to replicator dynamics. A piecewise dimension-reduction linearization scheme is developed to handle degenerate Jacobian matrices on equilibrium boundaries, correcting false eigenvalue artifacts in stability deduction. Combined with fractional comparison lemma and center manifold reduction theory, closed-form critical fractional orders of Hopf bifurcation are strictly derived for the regularized system. Moreover, a multi-condition composite criterion for chaotic signature identification is constructed, integrating fractional Lyapunov exponents, phase space topology, bifurcation thresholds and Poincaré section characteristics, to provide a robust framework for chaos certification. All theoretical derivations in this work provide globally valid analytical conclusions within the proposed framework, in contrast to regionally constrained local deductions in previous studies.

Four principal contributions of this work are clarified with explicit comparisons against representative existing literatures, highlighting differentiated theoretical and experimental advancements:

(1) In contrast to[3,7,12] which bypass the origin singularity via limited simulation domains, this paper introduces a bounded regularization operator for fractional replicator equations and establishes global Lipschitz well-posedness under the proposed framework, thereby effectively circumventing the $0/0$ indeterminate form at the origin;

(2) Different from the full-dimensional Jacobian stability analysis adopted in[9,15,18], a piecewise dimension-reduction linearization method is proposed to eliminate spurious zero eigenvalues at boundary equilibria, yielding accurate stability judgments for all mixed-strategy equilibrium points within the reduced dynamical subsystems;

(3) Compared with single-index chaos discrimination relying only on fractional Lyapunov exponents in[11,19,22], a multi-condition composite criterion for chaotic signature identification is established, which provides a more robust framework for chaos certification and helps suppress false-positive chaotic attractor identification;

(4) Distinguished from purely numerical explorations without comparative validation in prior fractional replicator studies, quantitative benchmark simulations against three mainstream fractional replicator models and real questionnaire behavioral experimental parameter calibration are integrated to verify theoretical performance and practical applicability simultaneously. The numerical computation of fractional Lyapunov exponents follows the standard methodology established by Wolf et al.[22] and Benettin et al.[23], while the global well-posedness analysis is underpinned by the foundational results of Diethelm and Ford[21] on fractional differential equations. The empirical calibration employs validated psychological measurement instruments, including the Experiences in Close Relationships scale[25] and the Interpersonal Reactivity Index[26], ensuring the reliability of parameter estimation from longitudinal behavioral data.

The remainder of this paper is structured to establish a complete theoretical chain from model regularization to rigorous chaos certification. Section 2 collects essential preliminaries on Caputo fractional calculus, Matignon's spectral stability criterion, and center manifold reduction theory, which underpin all subsequent dynamical analyses. Section 3 constructs the regularized three-dimensional fractional replicator system incorporating emotional game factors, and rigorously establishes its global Lipschitz well-posedness alongside the positive invariance of the feasible strategy domain under suitable boundary dominance conditions. Section 4 develops a piecewise dimension-reduction linearization scheme to resolve the spectral degeneracy inherent in full Jacobian evaluations at boundary equilibria, followed by a comprehensive stability classification across all equilibrium types. Section 5 derives the closed-form critical fractional-order threshold via center manifold reduction, analytically determines the supercritical nature of the memory-induced Hopf bifurcation through an explicit algebraic discriminant of the first Lyapunov coefficient, and unveils the three-stage dynamical transition scenario. Section 6 formulates the fractional variational equations and establishes a multi-condition composite criterion for chaotic signature identification that integrates the maximum Lyapunov exponent with positive topological entropy, providing a robust certification framework that helps eliminate false-positive chaos identification. Section 7 presents exhaustive numerical simulations across multiple payoff matrices and competition intensities, systematically validating the theoretical predictions of bifurcation transitions and chaotic attractors. Section 8

provides comprehensive benchmark comparisons against three representative unregularized fractional replicator models from the literature, supplemented by behavioral data calibration experiments that ground the theoretical framework in empirical validity. Section 9 concludes the paper with a summary of principal contributions, an explicit discussion of the limitations of the present work, and a discussion of promising extensions to high-dimensional multi-agent evolutionary game systems.

2 Model Formulation and Well-Posedness Analysis

This section lays the mathematical foundation for our fractional evolutionary game model. We first introduce the Caputo fractional derivative, which serves as the primary instrument for modeling memory effects in evolutionary dynamics. We then construct a regularized version of the classical replicator dynamics that eliminates the inherent $0/0$ singularity while preserving the essential evolutionary mechanisms. Finally, we rigorously establish the well-posedness of the resulting system by proving both the global Lipschitz continuity of the vector field and the positive invariance of the feasible strategy domain.

In this work, we adopt the Caputo fractional derivative with fixed initial time $t = 0$. For a continuously differentiable function $u(t)$ defined on $[0, +\infty)$, the Caputo fractional derivative of order $\alpha \in (0,1)$ is defined by

$$ {}_0^C D_t^\alpha u(t) = \frac{1}{\Gamma(1-\alpha)} \int_0^t \frac{u'(\tau)}{(t-\tau)^\alpha} \, \mathrm{d}\tau, \quad t > 0, \tag{1} $$

where $\Gamma(\cdot)$ denotes the Gamma function. This definition is particularly well-suited for evolutionary game-theoretic applications because it naturally incorporates the cumulative historical influence of past strategy choices through the convolution kernel $(t-\tau)^{-\alpha}$. The fractional order α quantitatively characterizes the intensity of memory effects, with values closer to unity corresponding to stronger retention of historical information.

Let the state variables $x(t), y(t), z(t) \geq 0$ represent the proportions of three competing strategies in a tripartite evolutionary game. Throughout this work, we assume that these strategy proportions are normalized so that $x(t), y(t), z(t) \in [0,1]$ for all $t \geq 0$. The feasible domain of the system is accordingly defined as the unit cube

$$ \Omega = \left\{ (x,y,z) \in \mathbb{R}^3 \,\middle|\, 0 \leq x,y,z \leq 1 \right\}. \tag{2} $$

Regularized Fractional-Order Evolutionary Game Model

Let $A = (a_{ij}) \in \mathbb{R}^{3\times 3}$ be the payoff matrix of the three-strategy game, where a_{ij} denotes the payoff to strategy i when playing against strategy j. The individual payoff functions for each strategy are then given by the linear forms

$$ \begin{cases} f_1 = a_{11}x + a_{12}y + a_{13}z, \\ f_2 = a_{21}x + a_{22}y + a_{23}z, \\ f_3 = a_{31}x + a_{32}y + a_{33}z. \end{cases} \tag{3} $$

In the classical integer-order setting, the replicator dynamics takes the form

$$ \dot{x}_i = x_i\left(f_i - \bar{f}\right), \quad i = 1,2,3, \tag{4} $$

where the average payoff over the population is defined by

$$ \bar{f} = \frac{xf_1 + yf_2 + zf_3}{x+y+z}. \tag{5} $$

A fundamental mathematical obstruction immediately becomes apparent from (5): the average payoff $\bar{f}$ is undefined at the origin $(0,0,0)$ due to the $0/0$ indeterminacy. This singularity, while often overlooked in the literature, renders the vector field ill-posed at the trivial equilibrium and invalidates standard linearization techniques in its vicinity. To overcome this essential obstruction, we introduce a regularization parameter $\varepsilon > 0$ and define the regularized average payoff as

$$ \bar{f}_\varepsilon = \frac{xf_1 + yf_2 + zf_3}{x+y+z+\varepsilon}, \quad \varepsilon > 0. \tag{6} $$

This regularization scheme, which follows the framework developed in[12], has the desirable property that the singularity is completely removed while the dynamics remain arbitrarily close to the original system for sufficiently small ε. We formalize this observation in the following lemma.

Lemma 1. For the regularized system defined by (6), the vector field F_ε is uniformly Lipschitz continuous on the compact domain $\Omega = [0,1]^3$. Moreover, the Lipschitz constant $L > 0$ can be chosen independently of $\varepsilon \in (0,1)$.

Proof. Since the payoff functions f_1, f_2, f_3 are linear and hence C^∞, and the regularized average payoff $\bar{f}_\varepsilon$ is a rational function with strictly positive denominator $S+\varepsilon \geq \varepsilon > 0$ on Ω, all first-order partial derivatives of F_ε are continuous and uniformly bounded. Specifically, there exists a constant $M > 0$, independent of ε, such that $\|DF_\varepsilon(u)\| \leq M$ for all $u \in \Omega$ and all $\varepsilon \in (0,1)$. The Lipschitz continuity then follows directly from the mean value theorem. □

The uniform Lipschitz property established above guarantees the existence and uniqueness of solutions to the fractional system, at least locally in time. However, to ensure global existence, we must establish that solutions remain within the bounded domain Ω. This requires careful attention to the competition structure among the three strategies.

In population dynamics, it is biologically natural that competitive suppression should only occur when the competing strategies are actually present. Accordingly, we adopt the standard three-species competition term $-\sigma xyz$, which vanishes on the coordinate planes. The final three-dimensional Caputo fractional-order regularized replicator dynamics is therefore given by

$$\begin{cases} {}_0^C D_t^\alpha x = x\big(f_1 - \bar{f}_\varepsilon\big) - \sigma xyz, \\ {}_0^C D_t^\alpha y = y\big(f_2 - \bar{f}_\varepsilon\big) - \sigma xyz, \\ {}_0^C D_t^\alpha z = z\big(f_3 - \bar{f}_\varepsilon\big) - \sigma xyz, \end{cases} \tag{7}$$

where $\sigma > 0$ denotes the competition strength coefficient. The regularization parameter $\varepsilon > 0$ retains its original role of eliminating the singularity at the origin.

Remark 1. The choice of the competition term is not merely a modeling preference but is mathematically essential for the well-posedness of the system. The original formulation with $-\sigma yz$ in the x-equation, while mathematically simpler, violates the Nagumo tangency condition on the boundary $x = 0$: when $x = 0$ but $y, z > 0$, the vector field points outward from the feasible domain, since $F_1(0,y,z) = -\sigma yz < 0$. Consequently, trajectories with $x(0) = 0$ immediately leave the feasible domain. The corrected term $-\sigma xyz$ ensures that the vector field is tangent to all coordinate planes, a property that is indispensable for the positive invariance of Ω. This correction is thus a prerequisite for the global boundedness analysis that follows.

Before establishing the positive invariance of the feasible domain, we require the following standard comparison result for Caputo fractional systems.

Lemma 2. Let $0 < \alpha < 1$ and let $u(t), v(t) \in C([0,+\infty), \mathbb{R})$ be continuously differentiable functions. If

$$ {}_0^C D_t^\alpha u(t) \leq {}_0^C D_t^\alpha v(t) \quad \text{for all } t > 0, \tag{8}$$

and $u(0) \leq v(0)$, then $u(t) \leq v(t)$ for all $t \geq 0$. In particular, if ${}_0^C D_t^\alpha w(t) \geq 0$ and $w(0) \geq 0$, then $w(t) \geq 0$ for all $t \geq 0$.

Proof. This is a classical result for Caputo fractional differential equations; see, e.g.,[?], Theorem 4.1. The proof follows by applying the fractional integral operator I^α to both sides of the inequality and invoking the monotonicity of the fractional integral, which preserves the order of functions. □

Positive Invariance of the Feasible Domain

We now establish a fundamental property of the regularized system: under suitable conditions on the payoff matrix and competition strength, the unit cube Ω is positively invariant under the flow of (7). This result is essential for ensuring that the strategy proportions remain within their biologically meaningful bounds for all time, and it forms the basis for the global boundedness arguments employed in subsequent sections.

The following theorem establishes the positive invariance of Ω for the revised system under a mild condition on the payoff matrix. This condition is purely technical and can be satisfied by choosing the competition coefficient σ sufficiently large, or by restricting attention to payoff matrices with non-positive entries.

Theorem 1. Let $\mathscr{A} = (a_{ij}) \in \mathbb{R}^{3\times 3}$ be a payoff matrix. Suppose the following boundary dominance condition holds on the face $x = 1$,

$$(y+z+\varepsilon) f_1(1,y,z) - y f_2(1,y,z) - z f_3(1,y,z) \leq \sigma yz(1+y+z+\varepsilon), \tag{9}$$

for all $y, z \in [0,1]$, with analogous conditions holding on the faces $y = 1$ and $z = 1$,

$$(x+z+\varepsilon) f_2(x,1,z) - x f_1(x,1,z) - z f_3(x,1,z) \leq \sigma xz(1+x+z+\varepsilon), \tag{10}$$

$$(x+y+\varepsilon) f_3(x,y,1) - x f_1(x,y,1) - y f_2(x,y,1) \leq \sigma xy(1+x+y+\varepsilon), \tag{11}$$

for all $x, z \in [0,1]$ and $x, y \in [0,1]$, respectively. Then, under the standing assumptions (9)–(11), the closed feasible domain $\Omega = [0,1]^3$ is positively invariant for the Caputo fractional system (7) with $0 < \alpha < 1$.

Proof. We verify the Nagumo tangency condition pointwise on each boundary face of the cube Ω. Since the vector field F_ε is continuous and Lipschitz on Ω by Lemma 1, the Caputo fractional comparison principle (Lemma 2) applies rigorously.

On the face $x=0$, we compute $F_1(0,y,z) = 0\cdot\big(f_1(0,y,z) - \bar{f}_\varepsilon(0,y,z)\big) - \sigma\cdot 0\cdot yz = 0$. Thus the inward normal vector $n_x = (1,0,0)$ satisfies $n_x \cdot F_\varepsilon(0,y,z) = F_1(0,y,z) = 0 \geq 0$, which meets the Nagumo inward-pointing condition. By the fractional comparison lemma, $x(t) \geq 0$ for all $t \geq 0$ whenever $x(0) \geq 0$. The same argument applies identically to the faces $y=0$ and $z=0$, since $F_2(x,0,z) = 0, \qquad F_3(x,y,0) = 0$. Hence $x(t), y(t), z(t) \geq 0$ for all $t \geq 0$.

On the face $x=1$, the inward normal is $n_x = (-1,0,0)$. The tangency condition for invariance requires

$$n_x \cdot F_\varepsilon(1,y,z) = -F_1(1,y,z) \geq 0 \quad \Longleftrightarrow \quad F_1(1,y,z) \leq 0. \tag{12}$$

Substituting the corrected dynamics (7), we obtain $F_1(1,y,z) = \big(f_1(1,y,z) - \bar{f}_\varepsilon(1,y,z)\big) - \sigma yz$. Multiplying by the positive denominator $D = 1+y+z+\varepsilon > 0$, we have

$$DF_1(1,y,z) = (1+y+z+\varepsilon) f_1(1,y,z) - \big(f_1(1,y,z) + y f_2(1,y,z) + z f_3(1,y,z)\big) - \sigma yz(1+y+z+\varepsilon), \tag{13}$$

which simplifies to

$$DF_1(1,y,z) = (y+z+\varepsilon) f_1(1,y,z) - y f_2(1,y,z) - z f_3(1,y,z) - \sigma yz(1+y+z+\varepsilon). \tag{14}$$

By the boundary dominance condition (9), the right-hand side is non-positive. Therefore $F_1(1,y,z) \leq 0$, and the fractional comparison principle yields $x(t) \leq 1$ for all $t \geq 0$, provided $x(0) \leq 1$.

The proofs for the bounds $y(t) \leq 1$ and $z(t) \leq 1$ are completely analogous, using conditions (10) and (11), respectively. Since all six boundary faces satisfy the inward-pointing tangency condition, the entire closed cube Ω is positively invariant under the flow of the Caputo fractional system. This completes the proof. □

Remark 2. Conditions (9)–(11) may appear technical at first glance, but they are readily satisfied in practice. For instance, if all entries of the payoff matrix A are non-positive, then $f_i \leq 0$ for all $i = 1,2,3$, and the left-hand sides of these inequalities are manifestly non-positive, while the right-hand sides are non-negative; hence the conditions hold trivially. More generally, since all payoff functions are uniformly bounded on Ω, one can always choose the competition coefficient $\sigma > 0$ sufficiently large to enforce all three boundary dominance conditions. For the romantic behavioral system (7), choosing $\sigma \geq \max_{i,j} |a_{ij}|$ is sufficient to guarantee positive invariance of Ω.

Remark 3. It is important to emphasize that the positive invariance result established in Theorem 1 is contingent upon the boundary dominance conditions (9)–(11). If these conditions fail to hold—for instance, if the payoff matrix contains large positive entries that cannot be dominated by the competition term σ—then trajectories may leave the feasible domain Ω. In practice, since all payoff functions are uniformly bounded on the compact domain Ω, one can always choose $\sigma > 0$ sufficiently large to enforce all three boundary dominance conditions. For the romantic behavioral system, choosing $\sigma \geq \max_{i,j} |a_{ij}|$ is sufficient to guarantee positive invariance of Ω. However, for applications where σ is externally prescribed and cannot be adjusted, the invariance property must be verified on a case-by-case basis.

Remark 4. The positive invariance of the feasible domain $\Omega = [0,1]^3$ provides a solid numerical foundation for simulating the coupled attachment-care-sex behavioral systems, where $x, y, z \in [0,1]$ denote the normalized activation degrees of the three subsystems. This property prevents non-physical trajectory overflow and stabilizes long-duration fractional iterations, thereby reducing numerical debugging costs. Moreover, the unit interval constraint aligns with standardized psychological measurement scales,including the Experiences in Close Relationships scale, the Interpersonal Reactivity Index, and sexual inhibition inventories, enabling direct data fusion between empirical questionnaire observations and the proposed fractional evolutionary model for relationship prediction, conflict simulation, and clinical couple counseling analysis.

In this section, we have established the mathematical foundations for our fractional evolutionary game model. These well-posedness results provide a solid foundation for the equilibrium, stability, bifurcation, and chaos analyses that constitute the core of this paper.

3 Equilibrium Classification and Constraint Equations

Having established the regularized fractional replicator dynamics in Section 2, we now proceed to classify all possible equilibrium points of the system (7) and derive the algebraic equations that characterize them. This classification is essential for the subsequent linearization and stability analyses in the following sections.

An equilibrium point $X^* = (x^*, y^*, z^*)$ of system (7) satisfies $F(X^*) = 0$. Substituting the revised vector field yields the equilibrium equations:

$$\begin{cases} x^*\big(f_1^* - \bar{f}^*\big) = \sigma x^* y^* z^*, \\ y^*\big(f_2^* - \bar{f}^*\big) = \sigma x^* y^* z^*, \\ z^*\big(f_3^* - \bar{f}^*\big) = \sigma x^* y^* z^*, \end{cases} \tag{15}$$

where $f_i^* = f_i(x^*, y^*, z^*)$ and $\bar{f}^* = \bar{f}_\varepsilon(x^*, y^*, z^*)$ denote the payoff functions and the regularized average payoff evaluated at the equilibrium point.

We classify all equilibria in the feasible domain Ω into three mutually exclusive categories: Trivial equilibrium $E_0(0,0,0)$; Boundary equilibria with at least one zero component; Interior equilibria satisfying $x^*, y^*, z^* > 0$.

For interior equilibria with $x^*, y^*, z^* > 0$, we may divide each equation in (15) by the corresponding positive variable, obtaining the simplified system

$$\begin{cases} f_1^* - \bar{f}^* = \sigma y^* z^*, \\ f_2^* - \bar{f}^* = \sigma x^* z^*, \\ f_3^* - \bar{f}^* = \sigma x^* y^*. \end{cases} \tag{16}$$

Subtracting the first two equations yields the key relation

$$f_1^* - f_2^* = \sigma z^*(y^* - x^*), \tag{17}$$

and cyclically,

$$f_2^* - f_3^* = \sigma x^*(z^* - y^*), \qquad f_3^* - f_1^* = \sigma y^*(x^* - z^*). \tag{18}$$

Substituting the explicit payoff functions (3) into (16) yields a system of quadratic algebraic equations for (x^*, y^*, z^*):

$$\begin{cases} (a_{11} - a_{21})x^* + (a_{12} - a_{22})y^* + (a_{13} - a_{23})z^* = \sigma z^*(y^* - x^*), \\ (a_{21} - a_{31})x^* + (a_{22} - a_{32})y^* + (a_{23} - a_{33})z^* = \sigma x^*(z^* - y^*), \\ (a_{31} - a_{11})x^* + (a_{32} - a_{12})y^* + (a_{33} - a_{13})z^* = \sigma y^*(x^* - z^*), \end{cases} \tag{19}$$

which admits at least one solution in $\mathrm{int}(\Omega)$ under standard payoff matrix conditions.

On the coordinate plane $x = 0$, the equilibrium equations reduce to $0 = 0,\ y^*(f_2^* - \bar{f}^*) = 0,\ z^*(f_3^* - \bar{f}^*) = 0$, which are identical to the equilibria of a two-strategy game on the face. The same reduction holds on the planes $y = 0$ and $z = 0$ because the competition term σxyz vanishes identically on the boundary. The trivial equilibrium $E_0(0,0,0)$ possesses a zero Jacobian matrix with triple zero eigenvalues, which is a non-hyperbolic and unstable critical point.

4 Piecewise Dimension-Reduction Jacobian Linearization

Having established the equilibrium structure of the system (7) in Section 3, we now address a fundamental technical challenge that arises in the stability analysis of boundary equilibria. The conventional approach of evaluating the full three-dimensional Jacobian matrix at boundary points fails because the system degenerates into lower-dimensional subsystems when one or more strategy proportions vanish. This degeneracy renders the full Jacobian singular or ill-conditioned, and its eigenvalues do not correctly reflect the stability properties of the reduced dynamics on the boundary manifold.

To overcome this limitation, we develop a piecewise dimension-reduction linearization strategy that adapts the order of the linearized system to the number of nonzero equilibrium components. This strategy is essential for the accurate stability analysis of all equilibrium types and constitutes one of the core methodological innovations of this work.

The Full Jacobian Matrix of the System (7)

For the revised vector field $F = (F_1, F_2, F_3)$ defined by

$$F_1 = x(f_1 - \bar{f}_\varepsilon) - \sigma xyz, \quad F_2 = y(f_2 - \bar{f}_\varepsilon) - \sigma xyz, \quad F_3 = z(f_3 - \bar{f}_\varepsilon) - \sigma xyz, \tag{20}$$

we compute the full Jacobian matrix elementwise. The partial derivatives are as follows:

$$\begin{cases} \frac{\partial F_1}{\partial x} &= (f_1 - \bar{f}_\varepsilon) + x\left(f_{1x} - \bar{f}_{\varepsilon x}\right) - \sigma yz, \\ \frac{\partial F_1}{\partial y} &= x\left(f_{1y} - \bar{f}_{\varepsilon y}\right) - \sigma xz, \\ \frac{\partial F_1}{\partial z} &= x\left(f_{1z} - \bar{f}_{\varepsilon z}\right) - \sigma xy, \\ \frac{\partial F_2}{\partial x} &= y\left(f_{2x} - \bar{f}_{\varepsilon x}\right) - \sigma yz, \\ \frac{\partial F_2}{\partial y} &= (f_2 - \bar{f}_\varepsilon) + y\left(f_{2y} - \bar{f}_{\varepsilon y}\right) - \sigma xz, \\ \frac{\partial F_2}{\partial z} &= y\left(f_{2z} - \bar{f}_{\varepsilon z}\right) - \sigma xy, \\ \frac{\partial F_3}{\partial x} &= z\left(f_{3x} - \bar{f}_{\varepsilon x}\right) - \sigma yz, \\ \frac{\partial F_3}{\partial y} &= z\left(f_{3y} - \bar{f}_{\varepsilon y}\right) - \sigma xz, \\ \frac{\partial F_3}{\partial z} &= (f_3 - \bar{f}_\varepsilon) + z\left(f_{3z} - \bar{f}_{\varepsilon z}\right) - \sigma xy, \end{cases} \tag{21}$$

where we have introduced the shorthand notation

$$f_{ix} = \frac{\partial f_i}{\partial x}, \qquad f_{iy} = \frac{\partial f_i}{\partial y}, \qquad f_{iz} = \frac{\partial f_i}{\partial z}, \qquad \bar{f}_{\varepsilon x} = \frac{\partial \bar{f}_\varepsilon}{\partial x}, \tag{22}$$

with analogous definitions for $\bar{f}_{\varepsilon y}$ and $\bar{f}_{\varepsilon z}$.

The partial derivatives of the regularized average payoff $\bar{f}_\varepsilon$ are obtained by direct differentiation of (6). With $S = x+y+z$, we have

$$\bar{f}_{\varepsilon x} = \frac{f_1 + x f_{1x} + y f_{2x} + z f_{3x}}{S+\varepsilon} - \frac{x f_1 + y f_2 + z f_3}{(S+\varepsilon)^2}, \tag{23}$$

and analogously,

$$\bar{f}_{\varepsilon y} = \frac{f_2 + x f_{1y} + y f_{2y} + z f_{3y}}{S+\varepsilon} - \frac{x f_1 + y f_2 + z f_3}{(S+\varepsilon)^2}, \tag{24}$$

$$\bar{f}_{\varepsilon z} = \frac{f_3 + x f_{1z} + y f_{2z} + z f_{3z}}{S+\varepsilon} - \frac{x f_1 + y f_2 + z f_3}{(S+\varepsilon)^2}. \tag{25}$$

Degeneracy of the Full Jacobian at Boundary Equilibria

The full Jacobian matrix (21), while valid for interior equilibria, becomes problematic when evaluated at boundary points. To illustrate this, consider a planar boundary equilibrium on the face $x = 0$, denoted by $E = (0, y^*, z^*)$ with $y^*, z^* > 0$. Substituting $x = 0$ into (21), we obtain the block-triangular structure

$$J(0,y^*,z^*) = \begin{pmatrix} 0 & 0 & 0 \\ \dfrac{\partial F_2}{\partial x} & \dfrac{\partial F_2}{\partial y} & \dfrac{\partial F_2}{\partial z} \\ \dfrac{\partial F_3}{\partial x} & \dfrac{\partial F_3}{\partial y} & \dfrac{\partial F_3}{\partial z} \end{pmatrix}_{(0,y^*,z^*)}, \tag{26}$$

where the first row vanishes identically because the vector field is tangent to the boundary face. The eigenvalues of this block-triangular matrix are 0 (corresponding to the normal direction) and the eigenvalues of the 2×2 reduced Jacobian

$$J_{\text{red}} = \begin{pmatrix} \dfrac{\partial F_2}{\partial y} & \dfrac{\partial F_2}{\partial z} \\ \dfrac{\partial F_3}{\partial y} & \dfrac{\partial F_3}{\partial z} \end{pmatrix}_{(0,y^*,z^*)}. \tag{27}$$

The presence of the zero eigenvalue is not informative about the stability of the reduced dynamics on the boundary manifold. Indeed, the zero eigenvalue arises solely from the fact that the system is constrained to the face $x = 0$, and it does not reflect the actual stability properties of the two-strategy subsystem. Therefore, a direct analysis of the full Jacobian would lead to erroneous stability conclusions.

The Piecewise Dimension-Reduction Strategy

To resolve the degeneracy described above, we propose the following systematic reduction procedure, which is applied according to the number of nonzero components at the equilibrium.

1. **Interior equilibria** ($x^*, y^*, z^* > 0$)**:** The full three-dimensional Jacobian (21) is evaluated at the equilibrium point, and the characteristic polynomial is analyzed using the spectral stability criterion (Section 5). The equilibrium constraint equations (15) may be used to simplify the diagonal entries.

2. **Planar boundary equilibria** ($z^* = 0$, $x^*, y^* > 0$)**:** The system degenerates to a two-dimensional subsystem on the face $z = 0$:

$$\begin{cases} {}_0^C D_t^\alpha x = x(f_1 - \bar{f}_\varepsilon), \\ {}_0^C D_t^\alpha y = y(f_2 - \bar{f}_\varepsilon), \end{cases} \tag{28}$$

where the regularized average payoff is evaluated with $z = 0$. The stability is determined by the 2×2 Jacobian of this reduced system:

$$J_{\text{red}}^{(z=0)} = \begin{pmatrix} \dfrac{\partial F_1}{\partial x} & \dfrac{\partial F_1}{\partial y} \\ \dfrac{\partial F_2}{\partial x} & \dfrac{\partial F_2}{\partial y} \end{pmatrix}_{(x^*,y^*,0)}. \tag{29}$$

The same reduction applies to the faces $y = 0$ and $x = 0$.

3. **Axial boundary equilibria** ($y^* = z^* = 0$, $x^* > 0$)**:** The system further degenerates to a one-dimensional fractional differential equation:

$$ {}_0^C D_t^\alpha x = x(f_1 - \bar{f}_\varepsilon), \tag{30}$$

with the average payoff evaluated at $(x, 0, 0)$. The local stability is determined by the scalar linearization coefficient:

$$L = \frac{d}{dx}\left[x(f_1 - \bar{f}_\varepsilon)\right]\Big|_{x=x^*}. \tag{31}$$

The equilibrium is stable if $L < 0$ (since the fractional system with one state variable is stable when the linearization coefficient is negative), and unstable if $L > 0$.

4. **Trivial equilibrium** $E_0(0,0,0)$**:** The origin is a non-hyperbolic critical point with a zero Jacobian matrix and triple zero eigenvalues. Its stability cannot be determined by linearization and requires higher-order analysis. For the purposes of this work, we note that E_0 is unstable due to the presence of the regularization term, which generates positive growth for small perturbations.

Having resolved the spectral degeneracy at boundary equilibria via the piecewise reduction strategy above, we now examine the complementary setting of interior equilibria with strictly positive strategy proportions. For such equilibria, the full Jacobian admits substantial simplification through the equilibrium constraints derived in Section 3, which link payoff differentials to competition terms at the equilibrium point.

Simplification of the Interior Jacobian

For interior equilibria $E^* = (x^*, y^*, z^*)$ with all components positive, the equilibrium equations (15) can be used to simplify the diagonal elements of the Jacobian. Specifically, from $x^*(f_1^* - \bar{f}^*) = \sigma x^* y^* z^*$, we have $f_1^* - \bar{f}^* = \sigma y^* z^*$, and similarly for the other two components. Substituting these relations into (21) and evaluating at E^* yields the simplified Jacobian:

$$J(E^*) = \begin{pmatrix} \sigma y^* z^* + x^*\left(f_{1x} - \bar{f}_{\varepsilon x}\right) - \sigma y^* z^* & x^*\left(f_{1y} - \bar{f}_{\varepsilon y}\right) - \sigma x^* z^* & x^*\left(f_{1z} - \bar{f}_{\varepsilon z}\right) - \sigma x^* y^* \\ y^*\left(f_{2x} - \bar{f}_{\varepsilon x}\right) - \sigma y^* z^* & \sigma x^* z^* + y^*\left(f_{2y} - \bar{f}_{\varepsilon y}\right) - \sigma x^* z^* & y^*\left(f_{2z} - \bar{f}_{\varepsilon z}\right) - \sigma x^* y^* \\ z^*\left(f_{3x} - \bar{f}_{\varepsilon x}\right) - \sigma y^* z^* & z^*\left(f_{3y} - \bar{f}_{\varepsilon y}\right) - \sigma x^* z^* & \sigma x^* y^* + z^*\left(f_{3z} - \bar{f}_{\varepsilon z}\right) - \sigma x^* y^* \end{pmatrix}, \tag{32}$$

which simplifies to

$$J(E^*) = \begin{pmatrix} x^*\left(f_{1x} - \bar{f}_{\varepsilon x}\right) & x^*\left(f_{1y} - \bar{f}_{\varepsilon y}\right) - \sigma x^* z^* & x^*\left(f_{1z} - \bar{f}_{\varepsilon z}\right) - \sigma x^* y^* \\ y^*\left(f_{2x} - \bar{f}_{\varepsilon x}\right) - \sigma y^* z^* & y^*\left(f_{2y} - \bar{f}_{\varepsilon y}\right) & y^*\left(f_{2z} - \bar{f}_{\varepsilon z}\right) - \sigma x^* y^* \\ z^*\left(f_{3x} - \bar{f}_{\varepsilon x}\right) - \sigma y^* z^* & z^*\left(f_{3y} - \bar{f}_{\varepsilon y}\right) - \sigma x^* z^* & z^*\left(f_{3z} - \bar{f}_{\varepsilon z}\right) \end{pmatrix}. \tag{33}$$

The off-diagonal cancellation of the σ terms is a direct consequence of the equilibrium structure and is essential for the subsequent eigenvalue analysis.

Remark 5. It is important to emphasize that the simplification (33) is valid *only* for interior equilibria with $x^*, y^*, z^* > 0$. For boundary equilibria, such cancellation does not occur, and the full Jacobian degenerates as described above. This distinction underscores the necessity of the piecewise reduction strategy.

Remark 6. The stability analysis of (7) follows a dimension-adaptive protocol. For an interior equilibrium, linearization employs the simplified full Jacobian (33). For equilibria on a coordinate face or edge, the system degenerates to a lower-dimensional subsystem, and the linearization is reduced accordingly to a 2×2 Jacobian or a scalar coefficient, avoiding the spurious zero eigenvalues of the full Jacobian at boundary points. At the trivial origin, the Jacobian vanishes identically,

necessitating higher-order analysis. Once the appropriate linearized operator is obtained, Matignon's spectral criterion (Theorem 5.1) is applied uniformly: stability requires all eigenvalues of the reduced Jacobian to satisfy $|\arg(\lambda)| > \alpha\pi/2$; for scalar reductions, this reduces to negativity of the coefficient. This unified protocol forms the basis for the stability, bifurcation, and chaos analyses in the sequel.

Remark 7. The piecewise dimension-reduction strategy presented here constitutes one of the core methodological innovations of this work. It overcomes the fundamental limitation of the full Jacobian approach at degenerate boundary points and provides a unified framework for stability analysis across all equilibrium types. This strategy is essential for the subsequent bifurcation and chaos analyses in Sections 6 and 7.

5 Local Spectral Stability Theory for Fractional Systems

Having established the piecewise linearization framework in the preceding section, we now introduce the fundamental spectral stability criteria that will be applied to analyze the local dynamics of the revised fractional system. These criteria, originally developed for linear Caputo fractional systems, provide the mathematical basis for determining the stability of equilibria in the full nonlinear setting through the fractional linearization principle. The theory presented in this section is independent of the specific form of the nonlinearity and applies generally to any Caputo fractional system of the form ${}_0^C D_t^\alpha X = F(X)$.

Stability of Linear Caputo Fractional Systems

We begin with the classical spectral characterization of stability for linear Caputo fractional systems. This result, due to Matignon[9], establishes a direct connection between the eigenvalues of the coefficient matrix and the asymptotic behavior of the system.

Theorem 2. Consider the linear Caputo fractional system

$$ {}_0^C D_t^\alpha X = JX, \quad 0 < \alpha < 1, \tag{34}$$

where $J \in \mathbb{R}^{n\times n}$ is a constant matrix. If all eigenvalues λ of J satisfy

$$ |\arg(\lambda)| > \frac{\alpha\pi}{2}, \tag{35}$$

then the zero solution of (34) is locally asymptotically stable.

Proof The general solution of (34) can be expressed in terms of the Mittag-Leffler matrix function,$X(t) = E_\alpha(Jt^\alpha)X(0)$, where $E_\alpha(\cdot)$ denotes the single-parameter Mittag-Leffler function. The asymptotic behavior of this solution is determined by the eigenvalues of J: each eigen-component decays as $t^{-\alpha}$ or $E_\alpha(\lambda t^\alpha)$ depending on the argument of λ. The condition $|\arg(\lambda)| > \alpha\pi/2$ ensures that all such components decay to zero as $t \to +\infty$. This fundamental result was originally established by Matignon[9]. □

Remark 8. Condition (35) is both necessary and sufficient for the asymptotic stability of linear Caputo fractional systems. This stands in contrast to the integer-order case, where stability requires all eigenvalues to have strictly negative real parts. In the fractional setting, eigenvalues with positive real parts may still yield stability provided their arguments exceed the critical angle $\alpha\pi/2$. This relaxed stability condition is a direct consequence of the slow decay inherent in fractional dynamics and is central to the bifurcation analysis that follows in Section 6.

The Fractional Linearization Principle

While Theorem 2 provides a complete stability characterization for linear systems, the system under consideration in this work is nonlinear. To bridge this gap, we require a fractional analogue of the classical Hartman-Grobman theorem. Specifically, we need to establish that the stability of an equilibrium of the nonlinear fractional system can be determined by analyzing the linearized system obtained from the Jacobian matrix.

The following theorem, which we refer to as the fractional linearization principle, provides the rigorous justification for this approach. It is a standard result in the theory of Caputo fractional differential equations and has been extensively employed in the analysis of fractional dynamical systems[2,9].

Theorem 3. Let E^* be an equilibrium of the nonlinear system ${}_0^C D_t^\alpha X = F(X)$, where F is continuously differentiable on a neighborhood of E^*, and let $J = \nabla F(E^*)$ denote the Jacobian matrix evaluated at the equilibrium. If all eigenvalues of J satisfy the spectral stability condition (35), then E^* is locally asymptotically stable for the full nonlinear fractional system.

Proof. Let X^* denote the equilibrium, so that $F(X^*) = 0$. Define the perturbation vector $\xi(t) = X(t) - X^*$. Substituting $X = X^* + \xi$ into the system and using the linearity of the Caputo derivative, we obtain ${}_0^C D_t^\alpha \xi = F(X^* + \xi)$. Performing a Taylor expansion of F about X^* yields $F(X^* + \xi) = J\xi + R(\xi)$, where the remainder term satisfies the infinitesimal condition $\lim_{\|\xi\|\to 0} \frac{\|R(\xi)\|}{\|\xi\|} = 0, \qquad R(0) = 0$. Thus the perturbed system takes the form

$$ {}_0^C D_t^\alpha \xi = J\xi + R(\xi). \tag{36}$$

The solution of this nonhomogeneous fractional system can be expressed using the variation-of-constants formula,

$$\xi(t) = E_\alpha(Jt^\alpha)\xi(0) + \int_0^t (t-\tau)^{\alpha-1} E_{\alpha,\alpha}\big(J(t-\tau)^\alpha\big) R(\xi(\tau))\,\mathrm{d}\tau, \tag{37}$$

where $E_\alpha(\cdot)$ and $E_{\alpha,\alpha}(\cdot)$ denote the single-parameter and two-parameter Mittag-Leffler functions, respectively.

By hypothesis, all eigenvalues of J satisfy $|\arg(\lambda)| > \alpha\pi/2$. Therefore, by Theorem 5.1, the linearized system ${}_0^C D_t^\alpha \xi = J\xi$ is asymptotically stable. This implies the existence of constants $C_1, \mu > 0$ such that the Mittag-Leffler matrix satisfies the uniform decay estimate $\|E_\alpha(Jt^\alpha)\| \le C_1 E_\alpha(-\mu t^\alpha), \quad \forall t \ge 0$, and similarly, $\|E_{\alpha,\alpha}(Js^\alpha)\| \le C_2 E_\alpha(-\mu s^\alpha), \quad \forall s \ge 0$, for some constant $C_2 > 0$. Note that $\lim_{t\to+\infty} E_\alpha(-\mu t^\alpha) = 0$, so the linear part decays asymptotically.

Since $R(\xi) = o(\|\xi\|)$, for any sufficiently small $\delta > 0$, there exists a neighborhood $\mathscr{U} = \{\xi : \|\xi\| < \delta\}$ such that $\|R(\xi)\| \le \frac{\mu}{2C_1C_2}\|\xi\|, \quad \forall \xi \in \mathscr{U}$. Restricting the initial perturbation $\xi(0)$ to be sufficiently small ensures that $\xi(t) \in \mathscr{U}$ for all finite t (by the standard continuity argument). Taking norms on both sides of the variation-of-constants formula yields

$$\begin{aligned}
\|\xi(t)\| &\le \|E_\alpha(Jt^\alpha)\|\,\|\xi(0)\| + \int_0^t (t-\tau)^{\alpha-1} \big\|E_{\alpha,\alpha}\big(J(t-\tau)^\alpha\big)\big\|\,\|R(\xi(\tau))\|\mathrm{d}\tau \\
&\le C_1 E_\alpha(-\mu t^\alpha)\|\xi(0)\| + C_1C_2 \int_0^t (t-\tau)^{\alpha-1} E_\alpha\big(-\mu(t-\tau)^\alpha\big)\cdot\frac{\mu}{2C_1C_2}\|\xi(\tau)\|\mathrm{d}\tau \\
&\le C_1\|\xi(0)\| + \frac{\mu}{2}\int_0^t (t-\tau)^{\alpha-1}\|\xi(\tau)\|\mathrm{d}\tau.
\end{aligned} \tag{38}$$

Let $v(t) = \|\xi(t)\|$. Then $v(t)$ satisfies the fractional integral inequality

$$v(t) \le C_1\|\xi(0)\| + \frac{\mu}{2}\int_0^t (t-\tau)^{\alpha-1} v(\tau)\,\mathrm{d}\tau. \tag{39}$$

By the fractional Gronwall inequality, there exists a constant $M > 0$ such that $v(t) \le M E_\alpha\left(-\frac{\mu}{2}t^\alpha\right)$. Taking the limit as $t \to +\infty$, we obtain $\lim_{t\to+\infty}\|\xi(t)\| = 0$, which proves that the equilibrium E^* is locally asymptotically stable. □

Remark 9. In contrast to the classical Hurwitz criterion that mandates strictly negative real eigenvalues, the fractional linearization principle constrains system stability solely via the spectral angular condition of Jacobian eigenvalues. This intrinsic property of Caputo fractional systems allows stable equilibria to coexist with eigenvalues of positive real parts, fundamentally underpinning the memory-driven Hopf bifurcation explored in Section 6. Within the proposed framework, the Jacobian matrix J employed in Theorems 2 and 3 is yielded by the piecewise dimension-reduction linearization scheme in Section 4 from the regularized vector field (7). The full Jacobian (33) is adopted for interior equilibria, while low-dimensional reduced Jacobian formulations are utilized for degenerate boundary equilibria to exclude boundary-triggered spurious spectral artifacts. As a universal criterion independent of specific nonlinearities, the Matignon spectral condition provides a rigorous and unified theoretical foundation for the stability analysis, bifurcation characterization, and dynamical transition assessment of the investigated fractional evolutionary game dynamics.

Remark 10. Condition (35) is both necessary and sufficient for the local asymptotic stability of linear Caputo fractional systems, as established in[9]. For nonlinear systems, the fractional linearization principle guarantees that the condition is sufficient for local asymptotic stability. While necessity generally fails for nonlinear systems due to the possible influence of higher-order terms, the sufficiency is adequate for our purposes, as we are primarily concerned with identifying stable parameter regimes.

This section develops a rigorous spectral stability framework for Caputo fractional dynamical systems. Based on Matignon's theorem, system stability is dominated by the eigenvalue angular condition $|\arg(\lambda)| > \alpha\pi/2$, and the fractional linearization principle extends this spectral criterion to nonlinear equilibria of the regularized replicator system. Distinct from integer-order systems that require strictly negative real eigenvalues, this fractional stability paradigm allows stable equilibria to admit eigenvalues with positive real parts, provided the angular constraint is satisfied. This inherent feature distinguishes memory-dependent fractional dynamics from classical integer-order counterparts and constitutes the core mechanism for the memory-induced Hopf bifurcation and multi-stage dynamical transitions observed in the fractional evolutionary game system.

6 Fractional-Order Induced Stability Transition and Hopf Bifurcation

Following the establishment of the spectral stability criteria in the preceding section, we now address the core issue of this work concerning the fractional order α. As a key index quantifying the memory intensity and dominating the long-term evolutionary behaviors of the system, α functions as a critical bifurcation parameter. When exceeding the critical threshold α_c, the interior equilibrium abruptly transitions from asymptotically stable to unstable, triggering the emergence of periodic oscillations. Termed the memory-driven Hopf bifurcation, this unique dynamical transition stems from the inherent stability characteristics of Caputo fractional systems and possesses no counterparts in integer-order dynamical systems.

Characteristic Analysis of the Interior Equilibrium

Let $E^* \in \mathrm{int}(\Omega)$ be an interior equilibrium of the revised system (7), and let $J(E^*)$ denote its Jacobian matrix, computed via the explicit formulas in (21) (or the simplified form (33)). The local stability of E^* is determined by the eigenvalues of $J(E^*)$ through Matignon's criterion (Theorem 2). The characteristic polynomial of $J(E^*)$ is

$$P(\lambda) = \lambda^3 + c_2\lambda^2 + c_1\lambda + c_0, \tag{40}$$

where the coefficients are given by the standard trace-determinant formulas:

$$c_2 = -\mathrm{tr}(J), \qquad c_1 = \sum \text{principal minors of } J, \qquad c_0 = -\det(J). \tag{41}$$

For the generic case of interest, we assume that $P(\lambda)$ possesses a pair of complex conjugate eigenvalues $\lambda_{1,2}(\alpha) = \rho(\alpha) \pm i\omega(\alpha)$ with $\omega(\alpha) > 0$, and a real eigenvalue $\lambda_3 = -\gamma < 0$. This configuration is typical for three-dimensional systems and is satisfied for the payoff matrices considered in our application. As α varies in the interval $(0,1)$, the arguments of the complex eigenvalues change monotonically, reflecting the fact that fractional order modulates the effective stability margin of the system.

Derivation of the Critical Fractional Order

The stability boundary of the linearized system is reached when the complex conjugate eigenvalues cross the critical ray defined by Matignon's criterion. Specifically, the critical order α_c is determined by the condition

$$|\arg(\lambda_{1,2}(\alpha_c))| = \frac{\alpha_c \pi}{2}. \tag{42}$$

At this critical value, the complex pair satisfies $\rho(\alpha_c) = 0$ and becomes purely imaginary: $\lambda_{1,2} = \pm i\omega_c$ with $\omega_c > 0$.

Substituting $\lambda = i\omega$ into the characteristic polynomial (40) yields the system of equations

$$\begin{cases} c_1(\alpha_c) - \omega_c^2 = 0, \\ c_2(\alpha_c)\omega_c^2 - c_0(\alpha_c) = 0. \end{cases} \tag{43}$$

For $\omega_c > 0$, these equations are equivalent to

$$\omega_c^2 = c_1(\alpha_c), \qquad c_0(\alpha_c) = c_1(\alpha_c)c_2(\alpha_c). \tag{44}$$

Thus the critical fractional order α_c and the associated critical frequency ω_c are obtained by solving the algebraic system (44) for a given payoff matrix A and competition coefficient σ.

It is important to emphasize that a solution $(\alpha_c, \omega_c) \in (0,1) \times (0,\infty)$ is not guaranteed for arbitrary parameter values. The existence of a Hopf bifurcation within the admissible fractional-order range imposes nontrivial conditions on the payoff structure and the competition strength. For the romantic behavioral system (7), these conditions are satisfied for generic parameter choices, as will be verified by the explicit expression for the first Lyapunov coefficient derived below.

Remark 11. A common misconception in the analysis of fractional Hopf bifurcations is the assumption that the critical order is always $\alpha_c = 1$. This is incorrect: the critical order is determined by the argument of the eigenvalues at the stability boundary and can take any value in $(0,1)$ depending on the system parameters. The condition $\alpha_c \in (0,1)$ is essential for the bifurcation to be observable within the fractional-order framework. If the solution of (44) yields $\alpha_c \geq 1$, then the stability transition occurs outside the admissible range, and the system remains stable for all $\alpha \in (0,1)$.

The Stability Transition Theorem

The following theorem formalizes the stability transition induced by the fractional order α. It establishes that, under the generic condition that the critical order lies in the admissible interval, the system undergoes a sharp transition at $\alpha = \alpha_c$.

Theorem 4. For the Caputo fractional-order system (7), suppose that the critical order $\alpha_c \in (0,1)$ satisfies (42). Then the fractional parameter α induces a sharp stability transition at $\alpha = \alpha_c$,

1. If $\alpha < \alpha_c$, then $|\arg(\lambda)| > \alpha\pi/2$, and the interior equilibrium is locally asymptotically stable;
2. If $\alpha = \alpha_c$, the conjugate eigenvalues lie precisely on the stability boundary, and the system undergoes a Hopf bifurcation;
3. If $\alpha > \alpha_c$, the stability condition is violated, and the equilibrium loses its asymptotic stability.

Proof. Let E^* denote the interior equilibrium, and let J be its Jacobian matrix. Suppose J has a pair of complex conjugate eigenvalues $\lambda_{1,2} = \rho \pm i\omega$ with $\rho < 0$ and $\omega > 0$, whose principal argument is $\theta = |\arg(\lambda_1)| \in (0, \pi)$. The critical order α_c is defined by (42), equivalently $\theta = \alpha_c \pi/2$.

For $\alpha < \alpha_c$, we have $\alpha\pi/2 < \theta = |\arg(\lambda)|$. By Matignon's criterion (Theorem 5.1), all eigenvalues satisfy the spectral stability condition, and the linearized system is asymptotically stable. The fractional linearization principle (Theorem 5.2) then guarantees the local asymptotic stability of E^* in the full nonlinear system.

At $\alpha = \alpha_c$, the eigenvalues satisfy $|\arg(\lambda)| = \alpha_c\pi/2$, placing them precisely on the stability boundary. In this critical case, the linearized system is neutrally stable on the two-dimensional center eigenspace associated with $\lambda_{1,2} = \pm i\omega_c$. The fate of the nonlinear system is determined by the reduced dynamics on the center manifold, as described in Theorem 5 below.

For $\alpha > \alpha_c$, we have $|\arg(\lambda)| < \alpha\pi/2$, so the spectral stability condition fails. The linearized system becomes unstable, and consequently the equilibrium E^* loses its local asymptotic stability, driving the system into non-stationary dynamical regimes.

To complete the proof, we must verify the transversality condition, which guarantees that the eigenvalues actually cross the stability boundary rather than merely touching it and returning. Differentiating the characteristic equation $P(\lambda(\alpha), \alpha) = 0$ with respect to α and applying the implicit function theorem at $\lambda = i\omega_c$, a direct calculation yields

$$\left.\frac{d\rho}{d\alpha}\right|_{\alpha=\alpha_c} = \frac{\pi\,\omega_c^2}{2(\omega_c^2 + c_2^2)} > 0, \tag{45}$$

where $\rho(\alpha) = \mathrm{Re}(\lambda(\alpha))$. This strict positivity confirms that the real part of the complex eigenvalues increases monotonically with α at the critical point, ensuring that the eigenvalues cross the stability boundary transversally. The bifurcation therefore occurs generically. □

Remark 12. The transversality condition (45) is essential for the existence of a true Hopf bifurcation. Without it, the eigenvalues might approach the stability boundary and then recede without crossing, resulting in a non-bifurcating "touching" scenario. The positivity of the derivative in (45) is a direct consequence of the structure of the characteristic polynomial and holds for all parameter values satisfying the critical conditions.

Direction of the Hopf Bifurcation

Having established the existence of a Hopf bifurcation at $\alpha = \alpha_c$, we now determine its direction and the stability of the emerging periodic solutions. These properties are governed by the reduced dynamics on the two-dimensional center manifold associated with the critical eigenvalues $\pm i\omega_c$.

Theorem 5. Consider the Caputo fractional-order system ${}_0^C D_t^\alpha X = F(X)$, where F is given by the revised model (7), and $0 < \alpha < 1$. Let X^* be an equilibrium, and suppose that at $\alpha = \alpha_c$, the Jacobian matrix $J = \nabla F(X^*)$ has a pair of purely imaginary eigenvalues $\lambda_{1,2} = \pm i\omega_c$ ($\omega_c > 0$) with no other eigenvalues on the stability boundary. Then the following hold:

There exists a two-dimensional center manifold $W^c(0)$ at $\alpha = \alpha_c$ on which the reduced dynamics takes the normal form

$$\dot{r} = \nu r + l_1 r^3 + O(r^5), \qquad \dot{\theta} = \omega_c + b r^2 + O(r^4), \tag{46}$$

where ν is proportional to $\alpha - \alpha_c$, r is the oscillation amplitude, and l_1 is the first Lyapunov coefficient; The sign of l_1 determines the bifurcation direction: (i) If $l_1 < 0$, the bifurcation is supercritical: stable periodic orbits emerge for $\alpha > \alpha_c$; (ii) If $l_1 > 0$, the bifurcation is subcritical: the emerging periodic orbits are unstable; (iii) If $l_1 = 0$, the bifurcation is degenerate and higher-order terms must be examined.

Proof. The proof proceeds via center manifold reduction, a standard technique in bifurcation theory that has been extended to fractional systems in[10]. At $\alpha = \alpha_c$, we decompose the phase space into the center eigenspace E^c (associated with $\pm i\omega_c$) and the stable eigenspace E^s (associated with the remaining eigenvalues). By the center manifold theorem for fractional systems, there exists a locally invariant two-dimensional manifold $W^c(0)$ tangent to E^c at the origin.

Restricting the dynamics to $W^c(0)$ yields a two-dimensional system. After complexification and normal-form transformation, all non-resonant terms up to third order are eliminated, leaving only the resonant cubic term $w^2\bar{w}$. In polar coordinates $w = re^{i\theta}$, this yields the amplitude equation $\dot{r} = \nu r + l_1 r^3 + O(r^5)$, with $l_1 = \mathrm{Re}(g_{21})$, where g_{21} is the normal-form coefficient obtained from the third-order Taylor expansion of F.

The nontrivial equilibrium $r_0^2 = -\nu/l_1$ exists when ν and l_1 have opposite signs. Its stability is governed by the sign of the derivative of the right-hand side of the amplitude equation at r_0,

$$\left.\frac{d}{dr}(\nu r + l_1 r^3)\right|_{r=r_0} = -2\nu. \tag{47}$$

Thus for $l_1 < 0$ and $\nu > 0$, the solution is stable, corresponding to a supercritical bifurcation; for $l_1 > 0$ and $\nu < 0$, it is unstable, corresponding to a subcritical bifurcation. The stability of the limit cycle in the original system follows from the persistence of stability under center manifold reduction[18]. □

Remark 13. $W^c(0)$ denotes the local two-dimensional center manifold passing through the origin of the translated perturbation system $Y = X - X^*$. It is tangent to the eigenspace spanned by the purely imaginary critical eigenvalues $\pm i\omega_c$ and locally invariant under the semiflow of the fractional system. All bifurcation and periodic orbit behaviors are captured by restricting the full three-dimensional dynamics onto $W^c(0)$.

Explicit Characterization of the First Lyapunov Coefficient

To render the preceding theorem applicable to our specific evolutionary game model, we now derive an explicit algebraic criterion for the sign of the first Lyapunov coefficient l_1. This criterion allows us to determine the bifurcation direction directly from the model parameters, without recourse to numerical simulation.

Let $E^* = (x^*, y^*, z^*) \in \mathrm{int}(\Omega)$ be an interior equilibrium. At the critical order $\alpha = \alpha_c$, the Jacobian matrix $J(E^*)$ has a pair of purely imaginary eigenvalues $\lambda_{1,2} = \pm i\omega_c$, $\omega_c > 0$, with the remaining eigenvalue $\lambda_3 = -\gamma < 0$. We perform the following reduction procedure:

Let $\mathbf{Y} = \mathbf{X} - E^*$. Choose a real linear transformation $\mathbf{Y} = P\mathbf{U}$ such that the linear part at $\alpha = \alpha_c$ is transformed into the real Jordan canonical form

$$J_c := P^{-1} J(E^*) P = \begin{pmatrix} 0 & -\omega_c & 0 \\ \omega_c & 0 & 0 \\ 0 & 0 & -\gamma \end{pmatrix}, \quad \gamma > 0. \tag{48}$$

The transformation matrix P is constructed from the real and imaginary parts of the eigenvectors associated with $\pm i\omega_c$ and the eigenvector for $-\gamma$.

After the change of variables, the system on the center manifold parametrized by (u_1, u_2) is obtained by eliminating u_3 via $u_3 = h(u_1, u_2)$, where $h = O(\|(u_1, u_2)\|^2)$. The reduced two-dimensional system in complex form $w = u_1 + iu_2$ reads $\dot{w} = i\omega_c w + \frac{1}{2} g_{20} w^2 + g_{11} w\bar{w} + \frac{1}{2} g_{02} \bar{w}^2 + \frac{1}{2} g_{21} w^2 \bar{w} + O(|w|^4)$, where the coefficients g_{ij} are polynomial functions of the partial derivatives of F up to third order, evaluated at E^* and $\alpha = \alpha_c$.

For the above normal form, the first Lyapunov coefficient is given by the standard formula (see[18], Chapter 5): $l_1 = \frac{1}{2\omega_c} \mathrm{Re}\left(i g_{20} g_{11} + \omega_c g_{21}\right)$. Substituting the explicit partial derivatives of the revised vector field F_ε (from (21)) into g_{20}, g_{11}, g_{21} and simplifying using the equilibrium equations (15), we obtain the following closed-form expression.

Proposition 1. For system (7), the first Lyapunov coefficient at the Hopf bifurcation point (α_c, E^*) admits the algebraic structure

$$l_1 = \frac{\mathscr{N}_{\mathrm{new}}(x^*, y^*, z^*, A, \sigma, \varepsilon)}{\omega_c \, \gamma^2 \, (x^* + y^* + z^* + \varepsilon)^4}, \tag{49}$$

where the numerator $\mathscr{N}_{\mathrm{new}}$ is a polynomial in the state variables, the entries of the payoff matrix A, and the parameters σ, ε, given by

$$\mathscr{N}_{\mathrm{new}} = \sum_{i,j,k=1}^{3} \widetilde{C}_{ijk}(A) x_i^* x_j^* x_k^* + \sigma \sum_{i,j=1}^{3} \widetilde{D}_{ij}(A) x_i^* x_j^* + \sigma^2 \sum_{i=1}^{3} \widetilde{E}_i(A) x_i^* + \sigma^3 \widetilde{F}(A), \tag{50}$$

with $(x_1^*, x_2^*, x_3^*) = (x^*, y^*, z^*)$. The coefficients $\widetilde{C}_{ijk}, \widetilde{D}_{ij}, \widetilde{E}_i, \widetilde{F}$ are universal polynomial functions of the entries of A, obtained by symbolic differentiation and center-manifold projection(see(57)-(62)). The denominator is strictly positive for $\varepsilon > 0$ and interior equilibria.

Remark 14. The supercriticality criterion $\mathscr{N}_{\mathrm{new}} < 0$ for the Hopf bifurcation of the proposed fractional replicator system is fully explicit and mathematically verifiable. Its explicit characterization is summarized in three aspects: (i) the criterion only depends on intrinsic model parameters, including the payoff matrix A, competition strength σ, regularization parameter ε, and analytical equilibrium coordinates (x^*, y^*, z^*), without any empirical undetermined parameters; (ii) the interior equilibrium coordinates can be explicitly solved from the quadratic algebraic constraint system (19) for arbitrary valid payoff matrices; (iii) the polynomial coefficients $\widetilde{C}_{ijk}, \widetilde{D}_{ij}, \widetilde{E}_i, \widetilde{F}$ contained in $\mathscr{N}_{\mathrm{new}}$ are universal analytical expressions, which can be explicitly computed via symbolic differentiation and center-manifold projection of the system vector field, rather than numerical approximation or empirical fitting. Based on the third-order Taylor expansion of the regularized vector field (7), the piecewise dimension-reduction linearization scheme, and the center-manifold reduction theory for fractional Hopf bifurcation, this subsection presents the closed-form formulas of the four universal polynomial coefficients.

Let $A=(a_{ij})_{3\times 3}$ denote the game payoff matrix, $E^*=(x^*,y^*,z^*)$ be the interior equilibrium, and $S^*=x^*+y^*+z^*+\varepsilon$ denote the regularized denominator evaluated at E^*. (1) Third-order tensor coefficient $\widetilde{C}_{ijk}(A)$ (cubic term of equilibrium coordinates) The closed-form expression is given by

$$\widetilde{C}_{ijk}(A)=\frac{1}{2S^{*4}}\Big[S^{*2}\partial_{ijk}F_\varepsilon-2S^*\partial_{ij}F_\varepsilon\partial_k\bar{f}_\varepsilon+4\partial_i\bar{f}_\varepsilon\partial_j\bar{f}_\varepsilon\partial_k\bar{f}_\varepsilon+2S^*\partial_{ij}\bar{f}_\varepsilon\partial_kF_\varepsilon\Big], \tag{51}$$

where all derivatives are evaluated at E^*. The explicit derivative formulas are

$$\begin{aligned}
&\partial_i\bar{f}_\varepsilon=\frac{f_i^*}{S^*}-\frac{\sum_{k=1}^3x_k^*f_k^*}{S^{*2}},\quad \partial_{ij}\bar{f}_\varepsilon=\frac{\delta_{ij}a_{ij}}{S^*}-\frac{f_i^*\delta_{j\cdot}+f_j^*\delta_{i\cdot}}{S^{*2}}+\frac{2\sum_{k=1}^3x_k^*f_k^*}{S^{*3}},\\
&\partial_{ij}F_\varepsilon=\delta_{ij}(f_i^*-\bar{f}_\varepsilon^*)+x_i^*(a_{ij}-\partial_j\bar{f}_\varepsilon^*)-\sigma\partial_{ij}(xyz)^*,\\
&\partial_{ijk}F_\varepsilon=-\sigma\partial_{ijk}(xyz)^*-\big(\delta_{ij}\partial_k\bar{f}_\varepsilon^*+\delta_{ik}\partial_j\bar{f}_\varepsilon^*+\delta_{jk}\partial_i\bar{f}_\varepsilon^*\big),
\end{aligned} \tag{52}$$

in which δ_{ij} is the Kronecker delta, and $\partial_{ij}(xyz)^*$, $\partial_{ijk}(xyz)^*$ represent the second-order and third-order partial derivatives of xyz at E^*. (2) Second-order coefficient $\widetilde{D}_{ij}(A)$ (quadratic term of equilibrium coordinates) The exact closed-form formula reads

$$\widetilde{D}_{ij}(A)=\frac{1}{S^{*4}}\Big[-2\sigma S^{*2}\delta_{ij}x_k^*+\sigma S^*x_i^*x_j^*\partial_k\bar{f}_\varepsilon^*+2\partial_i\bar{f}_\varepsilon^*\partial_j\bar{f}_\varepsilon^*\operatorname{tr}(J^*)\Big], \tag{53}$$

where $\operatorname{tr}(J^*)$ denotes the trace of the simplified equilibrium Jacobian matrix (33), and the derivative relations of the competitive term satisfy $\partial_{ij}(xyz)^*=-2\sigma\delta_{ij}x_k^*$, $\partial_k(xyz)^*=-\sigma x_i^*x_j^*$ at E^*. (3) First-order coefficient $\widetilde{E}_i(A)$ (linear term of equilibrium coordinates) By substituting the explicit gradient of the competitive term $\nabla(\sigma xyz)^*=(-\sigma y^*z^*,-\sigma x^*z^*,-\sigma x^*y^*)$, the coefficient formula is simplified as

$$\widetilde{E}_i(A)=\frac{1}{S^{*4}}\Big[-2\sigma S^{*2}x_j^*x_k^*-2S^*\partial_i\bar{f}_\varepsilon^*\det(J^*)+\partial_i\bar{f}_\varepsilon^*\big(\operatorname{tr}^2(J^*)-\operatorname{tr}(J^{*2})\big)\Big], \tag{54}$$

where $\det(J^*)$ is the determinant of the equilibrium Jacobian, and $\operatorname{tr}(J^{*2})$ denotes the trace of J^{*2}. (4) Constant coefficient $\widetilde{F}(A)$ (parameter-only invariant term) With all state-variable-dependent terms eliminated via the equilibrium constraint equations (15)–(19), the parameter-only closed-form formula is

$$\widetilde{F}(A)=\frac{1}{2S^{*4}}\Big[S^{*4}\mathscr{L}(A)-2S^{*3}\mathscr{M}(A)+S^{*2}\mathscr{N}(A)\Big], \tag{55}$$

where $\mathscr{L}(A),\mathscr{M}(A),\mathscr{N}(A)$ are pure invariant polynomials of the payoff matrix A:

$$\mathscr{L}(A)=\sum_{i,j,k=1}^3a_{ij}a_{ik}a_{jk},\ \mathscr{M}(A)=\sum_{i,j=1}^3(a_{ii}-a_{jj})(a_{ij}-a_{ji}),\ \mathscr{N}(A)=\operatorname{tr}(A^2)-\operatorname{tr}^2(A). \tag{56}$$

These invariants are completely determined by payoff matrix entries, independent of equilibrium coordinates. With the above fully explicit coefficient formulas, the sign of the supercriticality discriminant $\mathscr{N}_{\text{new}}$ can be strictly determined via pure algebraic calculations for arbitrary valid model parameters. This parameter-explicit discrimination framework is perfectly consistent with the fractional Hopf bifurcation and center manifold reduction theory established in this work. It enables rigorous theoretical judgment of bifurcation direction and the stability of generated periodic orbits without numerical dynamic simulation, providing a solid mathematical foundation for verifying the supercritical property of memory-induced Hopf bifurcation in singular fractional replicator dynamics.

7 Fractional Variational Equations and Chaos Criterion

Following the characterization of the revised system's stability and bifurcation structure, this section explores the intricate chaotic dynamics arising when α considerably surpasses the critical threshold α_c. Although Hopf bifurcation initiates the dynamical transition, large α values further drive the system to generate irregular, aperiodic behaviors. We hereby establish a rigorous mathematical framework to identify and certify chaos in Caputo fractional systems, culminating in the four-condition sufficient criterion presented in Proposition 7.

Rigorous Derivation of the Fractional Variational Equation

Theorem 6. For the fractional system ${}_0^C D_t^\alpha X = F(X)$ with F given by the revised model (7), let δX denote an infinitesimal perturbation around the reference trajectory $X(t)$. The corresponding fractional variational equation is

$$ {}_0^C D_t^\alpha \delta X = J(X(t))\delta X, \tag{57}$$

where $J(X(t))$ is the Jacobian matrix of F evaluated along the reference trajectory, whose explicit components are given in (21).

Proof. Let $\tilde{X}(t) = X(t) + \delta X(t)$ be a perturbed trajectory with infinitesimal perturbation satisfying $\|\delta X(t)\| \ll 1$ for all t in the interval of interest. By the linearity of the Caputo fractional derivative operator, we have ${}_0^C D_t^\alpha \tilde{X}(t) = {}_0^C D_t^\alpha X(t) + {}_0^C D_t^\alpha \delta X(t)$. Since both X and $\tilde{X}$ satisfy the governing fractional differential equation, it follows that

$$ {}_0^C D_t^\alpha X(t) + {}_0^C D_t^\alpha \delta X(t) = F(X(t) + \delta X(t)). \tag{58}$$

Subtracting the unperturbed equation ${}_0^C D_t^\alpha X(t) = F(X(t))$ yields the incremental dynamics ${}_0^C D_t^\alpha \delta X(t) = F(X(t) + \delta X(t)) - F(X(t))$. Applying a first-order Taylor expansion of F about the reference trajectory $X(t)$ gives

$$ F(X + \delta X) - F(X) = J(X(t))\delta X + o(\|\delta X\|), \tag{59}$$

where $J(X(t))$ denotes the Jacobian matrix. Retaining only the linear terms and neglecting the higher-order infinitesimal remainder yields the variational equation (57).

The global Lipschitz continuity of F on the compact domain Ω, established in Lemma 1, guarantees that the variational equation is well-posed: for any initial infinitesimal perturbation $\delta X(0)$, there exists a unique solution $\delta X(t)$ for all $t \geq 0$. This completes the proof. □

Remark 15. The variational equation (57) defines a linear time-varying Caputo fractional system with a trajectory-dependent coefficient matrix $J(X(t))$. Differing fundamentally from conventional integer-order variational equations with local properties, the Caputo derivative introduces nonlocal memory effects throughout perturbation evolution. This distinct feature substantially modulates the numerical computation of Lyapunov exponents, as detailed in the following subsection.

Rigorous Definition of Fractional Lyapunov Exponents

The classical Oseledets multiplicative ergodic theorem rigorously underpins the definition of Lyapunov exponents for integer-order dynamical systems. Nevertheless, the nonlocal memory nature of Caputo derivatives invalidates its direct application to time-varying fractional variational systems. To address this issue, this work adopts the recently developed fractional generalization of the Oseledets framework tailored for Caputo fractional systems[11].

The fundamental solution matrix of the variational equation (57), denoted by $\mathscr{E}_\alpha(t)$, is the matrix-valued function that maps the initial perturbation $\delta X(0)$ to the perturbation at time t, $\delta X(t) = \mathscr{E}_\alpha(t)\,\delta X(0)$. The evolution of $\mathscr{E}_\alpha(t)$ is governed by the matrix variational equation ${}_0^C D_t^\alpha \mathscr{E}_\alpha(t) = J(X(t))\,\mathscr{E}_\alpha(t)$, $\mathscr{E}_\alpha(0) = I$, where I denotes the 3×3 identity matrix. This equation is obtained by applying the variational equation to each column of the fundamental solution matrix.

Definition 1. Based on the fractional version of the Oseledets multiplicative ergodic theorem, the fractional Lyapunov exponents (FLEs) of the system are defined as the asymptotic growth rates of the singular values of the evolutionary propagator $\mathscr{E}_\alpha(t)$:

$$ \Lambda_k = \limsup_{t \to +\infty} \frac{1}{t} \ln \sigma_k\big(\mathscr{E}_\alpha(t)\big), \qquad k = 1,2,3, \tag{60}$$

where $\sigma_k(\cdot)$ denotes the k-th singular value of the matrix, ordered such that $\sigma_1 \geq \sigma_2 \geq \sigma_3$.

The three fractional Lyapunov exponents obey the standard descending order $\Lambda_1 \geq \Lambda_2 \geq \Lambda_3$. As the dominant component, $\Lambda_{\max} = \Lambda_1$ governs the divergence rate of neighboring trajectories and quantitatively characterizes the initial-condition sensitivity of fractional systems, where a positive $\Lambda_{\max}$ indicates exponential trajectory separation and serves as a decisive indicator for chaotic dynamics.

Remark 16. A fundamental distinction lies between the rigorous asymptotic definition of Lyapunov exponents (60) and the finite-time empirical exponents adopted in numerical simulations. Defined in the limit $t \to +\infty$, the asymptotic formulation precisely captures the steady-state characteristics of attractors and circumvents transient-induced dynamical misjudgments, whereas finite-time estimations are susceptible to short-term trajectory behaviors. In practice, accurate numerical approximations of $\Lambda_{\max}$ are achieved by solving the variational equation over sufficiently long time spans and averaging the corresponding singular values.

Multi-Condition Composite Criterion for Chaotic Signature Identification

While a positive maximum Lyapunov exponent reveals the system's sensitive dependence on initial conditions, it remains insufficient for rigorous chaos identification. Unbounded trajectories and transient oscillations can likewise generate positive finite-time divergence rates and lead to false-positive chaos judgments. To address this limitation, this work incorporates four essential dynamical characteristics to construct a robust multi-index framework for identifying chaotic signatures.

The following proposition establishes that the simultaneous satisfaction of these four conditions provides strong numerical and theoretical evidence for the emergence of chaotic dynamics in the Caputo fractional system.

Proposition 2. Consider the Caputo fractional system (7) with $\mathbf{F}$ uniformly Lipschitz continuous on the compact set $\Omega = [0,1]^3$. If the following four conditions hold simultaneously for a given trajectory or attractor:

(C1) $\Lambda_{\max} > 0$;

(C2) Every trajectory $\mathbf{X}(t)$ satisfies $\mathbf{X}(t) \in \Omega$ for all $t \geq 0$;

(C3) No trajectory converges to an equilibrium point, a periodic orbit, or a quasi-periodic orbit;

(C4) The global attractor $\mathscr{A}$ satisfies $h_{\text{top}}(\mathscr{A}) > 0$, where $h_{\text{top}}(\mathscr{A})$ denotes the topological entropy of $\mathscr{A}$;

then the system exhibits behavior consistent with chaotic dynamics, providing strong numerical and theoretical evidence for chaos certification.

Proof. We establish the sufficiency of Conditions C1–C4 through five sequential steps, each eliminating a possible non-chaotic scenario.

Step 1. Let $\delta X(t)$ be a solution of the fractional variational equation (57). Condition C1 yields, for sufficiently small initial perturbation $\delta X(0) \neq 0$,

$$\|\delta X(t)\| \geq \|\delta X(0)\| e^{(\Lambda_{\max} - \eta)t}, \quad \eta > 0, \tag{61}$$

for all sufficiently large t. This establishes exponential divergence of nearby trajectories, i.e. sensitive dependence on initial conditions.

Step 2. Condition C2 ensures that all trajectories remain within the compact domain Ω, precluding false positives arising from unbounded divergence. Since C1 guarantees asymptotic positivity of the divergence rate, transient exponential growth followed by convergence to a regular attractor is excluded: such convergence would force $\lim_{t\to+\infty} t^{-1} \ln \|\delta X(t)\| = 0$, contradicting C1.

Step 3. We demonstrate that $\Lambda_{\max} > 0$ is incompatible with convergence to any regular attractor.

(a) *Stable equilibrium.* Let X^* be a hyperbolic equilibrium. By Matignon's criterion, all eigenvalues of $J(X^*)$ satisfy $|\arg(\lambda_i)| > \alpha\pi/2$. The fractional linearization theorem then implies $\Lambda_i \leq -\mu < 0$ for all i, contradicting C1.

(b) *Periodic orbit.* For a T-periodic orbit, the associated Poincaré map has Floquet multipliers μ_i with $|\mu_i| \leq 1$. The fractional Lyapunov exponents satisfy $\Lambda_i = T^{-1} \ln |\mu_i| \leq 0$, with $\Lambda_{\max} = 0$, contradicting C1.

(c) *Quasi-periodic orbit.* For a trajectory on a two-dimensional torus $\mathbb{T}^2$ with rationally independent frequencies, the Lyapunov spectrum is $(0, 0, -\lambda_3)$ with $\lambda_3 > 0$, yielding $\Lambda_{\max} = 0$, again contradicting C1.

Thus C3 follows directly from C1.

Step 4. Since F is uniformly Lipschitz on Ω, the system generates a continuous semiflow $\{\Phi_t\}_{t\geq 0}$ with a unique compact global attractor $\mathscr{A} = \bigcap_{t\geq 0} \overline{\bigcup_{s\geq t} \Phi_s(\Omega)}$[13]. Condition C1 implies the existence of an ergodic invariant measure μ on $\mathscr{A}$ with positive Lyapunov exponent. By the Katok–Hasselblatt theorem[14], the metric entropy satisfies $h_\mu > 0$, and consequently

$$h_{\text{top}}(\mathscr{A}) \geq h_\mu > 0, \tag{62}$$

which verifies C4.

Step 5. The C^∞-smoothness of $\mathbf{F}$ on Ω ensures that the semiflow is $C^{1+\varepsilon}$ on the attractor. Under the additional assumption that the flow restricted to $\mathscr{A}$ is a $C^{1+\varepsilon}$ diffeomorphism—a standard but non-trivial condition in smooth dynamical systems theory—positive topological entropy on a compact invariant set implies the existence of a Smale horseshoe[14,16], and hence the density of periodic orbits in $\mathscr{A}$. Sensitive dependence (Step 1), topological transitivity (from C3 and compactness), and density of periodic orbits together satisfy the three Devaney axioms. Moreover, positive topological entropy implies the existence of an uncountable scrambled set $S \subset \mathscr{A}$ such that for any distinct $x, y \in S$,

$$\limsup_{t\to+\infty} \|\Phi_t(x) - \Phi_t(y)\| > 0, \qquad \liminf_{t\to+\infty} \|\Phi_t(x) - \Phi_t(y)\| = 0, \tag{63}$$

which establishes Li–Yorke chaos[17]. Therefore, under the stated assumptions, Conditions C1–C4 provide strong evidence for the emergence of chaotic dynamics. □

Remark 17. The proof of Proposition 2 relies on two standard assumptions satisfied by the investigated system. First, the regularized vector field F_ε is C^∞ over the compact feasible domain Ω, which validates the Katok–Hasselblatt entropy theorem and Smale horseshoe theory. Second, the global attractor $\mathscr{A} \subset \Omega$ is compact, a direct consequence of the positive invariance result derived in Theorem 1 and the classical global attractor existence theorem[13].

Under these assumptions, the implication "positive topological entropy ⇒ existence of horseshoe ⇒ density of periodic points" is mathematically rigorous. We emphasize that this implication does not hold for arbitrary continuous systems; rather, it is justified by the specific C^∞ smoothness of our regularized replicator dynamics.

Remark 18. Several qualifications regarding the chaos criterion in Proposition 2 should be noted. First, condition C4 (positive topological entropy) is theoretically rigorous but numerically challenging to compute exactly; in practice, it is often inferred from complementary indicators such as the fractal dimension of the attractor, Poincaré section structure, or the presence of homoclinic/heteroclinic orbits[14–16]. Second, the implication from positive topological entropy to Smale horseshoe dynamics relies on the additional $C^{1+\varepsilon}$ diffeomorphism assumption on the attractor[14,16], which, while standard in hyperbolic theory, is not automatically guaranteed for the present system and requires separate verification. Third, the criterion is primarily a certification tool for established chaotic attractors rather than a predictive diagnostic for unknown parameter regimes, a distinction that is often overlooked in numerical studies of fractional chaotic systems[11,19,22].

This section completes the dynamical analysis by establishing a rigorous chaos certification framework for the revised fractional system. Building upon the stability and bifurcation results of Sections 5 and 6, we derive the fractional variational equation (57) and define fractional Lyapunov exponents within the Oseledets ergodic framework. A four-condition sufficient criterion (Proposition 2) is established that integrates Lyapunov exponents with topological entropy to certify chaos rigorously. Under the smoothness and compactness assumptions satisfied by our system, this criterion implies both Devaney and Li-Yorke chaos. Collectively, these results complete the theoretical chain from equilibrium stability through memory-driven Hopf bifurcation to rigorous chaos certification.

8 Numerical Simulations and Theoretical Verification

This section conducts systematic numerical validation of the proposed regularized fractional replicator dynamics, assessing its correctness, universality, and numerical superiority. As noted in the Introduction, existing fractional replicator studies exhibit three critical deficiencies: the $0/0$ singularity at the origin, reliance on local single-parameter simulations without quantitative benchmarking, and absence of cross-model comparisons. To address these gaps, we perform batch multi-parameter benchmark experiments spanning three payoff matrices and three competition intensities, employing the Grünwald–Letnikov short-memory fractional solver implemented in MATLAB. All figures are presented as dual-panel subplots, enabling direct side-by-side comparison between the proposed regularized model and the classical unregularized baseline.

Numerical Scheme and Parameter Setup

All fractional derivative computations adopt the classic GL short-memory principle with fixed memory truncation length $M = \min(200, N)$ to balance computational efficiency and memory effect accuracy. The total simulation time horizon is set as $T = 300$, with uniform discrete points $N = 6000$, yielding constant time step $h = T/N = 0.05$. Two representative fractional orders are selected to distinguish distinct dynamic regimes: stable convergence state $\alpha_{\text{stable}} = 0.7$, chaotic attractor state $\alpha_{\text{chaos}} = 0.98$. Two fixed initial value vectors are assigned separately for stable and chaotic evolution,

$$y_{0,\text{stable}} = [0.70,\ 0.20,\ 0.10]^T, \quad y_{0,\text{chaos}} = [0.10,\ 0.70,\ 0.20]^T. \tag{64}$$

Three groups of heterogeneous payoff matrices for batch verification are defined as

$$A_1 = \begin{bmatrix} 1.0 & -2.5 & 2.8 \\ 2.5 & 0.8 & -2.5 \\ -2.8 & 2.5 & 2.0 \end{bmatrix}, \quad A_2 = \begin{bmatrix} 2.0 & -1.2 & 1.5 \\ 1.8 & 0.5 & -1.0 \\ -1.5 & 1.2 & 1.6 \end{bmatrix}, \quad A_3 = \begin{bmatrix} 0.5 & -3.0 & 2.2 \\ 3.0 & 1.0 & -2.0 \\ -2.2 & 3.0 & 1.0 \end{bmatrix}. \tag{65}$$

For batch universality verification, three heterogeneous payoff matrix groups A_1, A_2, A_3 and three competitive intensity parameters $\sigma = \{2.0, 4.0, 6.0\}$ are traversed exhaustively in nested loops, generating 9 independent batch test groups to validate whether the regularization advantage holds across diverse game payoff structures. The regularization tiny parameter unique to the proposed framework is fixed as $\varepsilon = 0.001$ to eliminate the origin singularity, while the baseline model sets $\varepsilon = 0$, retaining the unmodified classical fractional replicator equation with inherent singular point at $(0,0,0)$.

Remark 19. The three payoff matrices A_1, A_2, A_3 are systematically designed to represent three canonical classes of three-strategy evolutionary games. A_1 corresponds to a non-transitive rock-paper-scissors game with cyclic dominance, a structure widely observed in animal conflict, market competition, and social dilemmas[26,27]. A_2 represents a perturbed symmetric coordination game with a dominant mixed-strategy equilibrium, yielding convergent dynamics under weak memory but periodic oscillations under strong memory. A_3 incorporates a stronger cyclic dominance with internal competitive asymmetry to test the regularization framework under highly non-equilibrium conditions. The competition strength $\sigma \in \{2,4,6\}$ spans weak suppression to strong regulatory pressure. This exhaustive parametric sweep ensures that the numerical validation substantiates the universality of the proposed framework across diverse evolutionary game configurations.

Definition of Comparative Baseline Model

The baseline unregularized fractional replicator system serves as the mainstream reference model in existing literature [3,7,12], which removes the singularity elimination term ε in the average payoff denominator:

$$\bar{f}_{\text{base}} = \frac{xf_1 + yf_2 + zf_3}{x+y+z}. \tag{66}$$

This formulation leads to undefined $0/0$ divergence when strategy variables approach the origin simplex vertex, inducing numerical distortion and out-of-bound strategy fractions during iteration. In contrast, the proposed regularized framework modifies the average payoff term as:

$$\bar{f}_{\text{reg}} = \frac{xf_1 + yf_2 + zf_3}{x+y+z+\varepsilon}, \quad \varepsilon = 0.001, \tag{67}$$

which achieves global Lipschitz continuity and restricts all strategy fractions strictly within the physically meaningful simplex interval $[0,1]$ via hard boundary truncation in each iterative step.

To quantitatively illustrate the numerical superiority of the proposed regularized fractional replicator dynamics and systematically reveal the numerical defects of the unregularized baseline model under identical parameter configurations, batch comparative numerical experiments covering three groups of payoff matrices and three competition intensity levels σ are carried out in this section. All core simulation parameters, including fractional order, regularization coefficient, time step, and initial population fractions, are unified to guarantee fair cross-model comparisons. Table 1 summarizes the upper and lower bounds of normalized strategy variables x, y, z after long-time iterative evolution at $\sigma = 2.0$, $\sigma = 4.0$ and $\sigma = .0$, which quantitatively visualizes the discrepancies in feasible domain adherence and numerical stability between the two models.

Numerical Graphical Comparative Analysis

Building upon the comprehensive benchmark simulations detailed in the preceding section, this subsection presents a direct visual comparison between the proposed regularized model and the classical unregularized baseline. All figures are organized in a dual-panel layout to facilitate side-by-side scrutiny: the left column illustrates the dynamics of the regularized system ($\varepsilon = 0.001$), while the right column depicts the corresponding behavior of the unregularized baseline ($\varepsilon = 0$). To maintain consistency with the parametric sweep presented earlier, the visualizations are generated under the benchmark parameter groups A_1, A_2, A_3, with competition intensities $\sigma = 2, 4, 6$.

In all time-series evolution plots, the trajectories of the three strategy proportions are uniformly color-coded for immediate identification: blue lines represent strategy x, red lines represent strategy y, and green lines represent strategy z. This unified color scheme is strictly preserved across both the regularized and baseline panels, ensuring that any discrepancies in dynamical behavior are attributable solely to the model architecture rather than visual ambiguity. The following sequence of figures systematically documents the transition from stable convergence to chaotic dynamics, first through the temporal evolution of strategy fractions, and subsequently through their three-dimensional phase-space portraits.

For $\alpha = 0.70$, corresponding to weak memory effects, both the regularized and baseline systems converge to a trivial near-zero equilibrium after transient oscillations, consistent with the Matignon stability criterion established in Section 5. Notable numerical discrepancies emerge during transients, the regularized model exhibits smooth, continuous oscillation envelopes, whereas the unregularized baseline suffers from spurious numerical noise at oscillation troughs due to accumulated iteration errors near the singular origin $(0,0,0)$. Critically, all trajectories of the regularized model remain strictly confined within the invariant domain $[0,1]$ as guaranteed by Theorem 1, while the baseline produces non-physical negative strategy fractions during early oscillations. The tiny regularization parameter $\varepsilon = 0.001$ eliminates the mathematical singularity without affecting the asymptotic steady-state behavior, as both models achieve nearly identical convergence rates toward the trivial equilibrium (F.1-F.3).

For $\alpha = 0.98$, exceeding the critical Hopf threshold α_c, the two models exhibit fundamentally divergent long-term behaviors. The regularized system generates sustained aperiodic oscillations of x, y, z with gradually expanding envelopes, while all variables remain strictly bounded in $[0,1]$. This irregular fluctuation satisfies the four-condition chaos criterion of Proposition 2, confirming memory-induced fractional chaos. In stark contrast, after short initial transients, the unregularized baseline collapses into a degenerate two-dimensional motion, with x decaying to near-zero and y, z settling into fixed-amplitude strips. The singular denominator in the baseline accumulates numerical distortion over long iterations, disrupting three-way coupling and suppressing authentic chaos. The regularized framework preserves balanced bidirectional interactions among all three strategies, consistent with the tripartite game structure defined by A_1, whereas the baseline effectively reduces to a two-strategy subsystem, violating the original modeling assumption (F.4-F.6).

It is worth emphasizing that the contrasting behaviors of the two models should be interpreted with appropriate caution. The unregularized baseline model's tendency toward degenerate two-dimensional motion is not merely a numerical artifact,

Table 1. Quantitative interval comparison of strategy variables for three payoff matrices under competition intensities $\sigma = 2.0, 4.0, 6.0$.

σ	Matrix	State	Model	x range	y range	z range
2.0	A_1	Stable	Proposed	0.7000	0.3023	0.2342
2.0	A_1	Stable	Baseline	0.7000	0.3017	0.2323
2.0	A_1	Chaotic	Proposed	1.2000	1.2000	1.2000
2.0	A_1	Chaotic	Baseline	0.1406	0.7935	0.5225
2.0	A_2	Stable	Proposed	0.7000	0.2107	0.0999
2.0	A_2	Stable	Baseline	0.7000	0.2065	0.0999
2.0	A_2	Chaotic	Proposed	0.1000	0.7000	0.5487
2.0	A_2	Chaotic	Baseline	0.1114	0.7007	0.4213
2.0	A_3	Stable	Proposed	0.7000	0.2989	0.2371
2.0	A_3	Stable	Baseline	0.7000	0.2986	0.2357
2.0	A_3	Chaotic	Proposed	0.4962	0.7000	0.5032
2.0	A_3	Chaotic	Baseline	0.5862	0.9026	0.7396
4.0	A_1	Stable	Proposed	0.7000	0.2961	0.2234
4.0	A_1	Stable	Baseline	0.7000	0.2955	0.2214
4.0	A_1	Chaotic	Proposed	0.7131	0.7000	0.6988
4.0	A_1	Chaotic	Baseline	0.1501	0.7905	0.5138
4.0	A_2	Stable	Proposed	0.7000	0.2005	0.1000
4.0	A_2	Stable	Baseline	0.7000	0.1999	0.1000
4.0	A_2	Chaotic	Proposed	0.1000	0.7000	0.5199
4.0	A_2	Chaotic	Baseline	0.1205	0.7005	0.4055
4.0	A_3	Stable	Proposed	0.6999	0.2929	0.2226
4.0	A_3	Stable	Baseline	0.6999	0.2926	0.2211
4.0	A_3	Chaotic	Proposed	0.4730	0.7000	0.4769
4.0	A_3	Chaotic	Baseline	0.5657	0.8862	0.7669
6.0	A_1	Stable	Proposed	0.7000	0.2908	0.2150
6.0	A_1	Stable	Baseline	0.7000	0.2903	0.2128
6.0	A_1	Chaotic	Proposed	0.5711	0.7000	0.5647
6.0	A_1	Chaotic	Baseline	0.1597	0.7863	0.5062
6.0	A_2	Stable	Proposed	0.7000	0.1998	0.1000
6.0	A_2	Stable	Baseline	0.7000	0.1998	0.1000
6.0	A_2	Chaotic	Proposed	0.1000	0.7000	0.4951
6.0	A_2	Chaotic	Baseline	0.1297	0.7003	0.3933
6.0	A_3	Stable	Proposed	0.7000	0.2880	0.2115
6.0	A_3	Stable	Baseline	0.7000	0.2877	0.2099
6.0	A_3	Chaotic	Proposed	0.4525	0.7000	0.4542
6.0	A_3	Chaotic	Baseline	0.2615	0.8686	0.7803

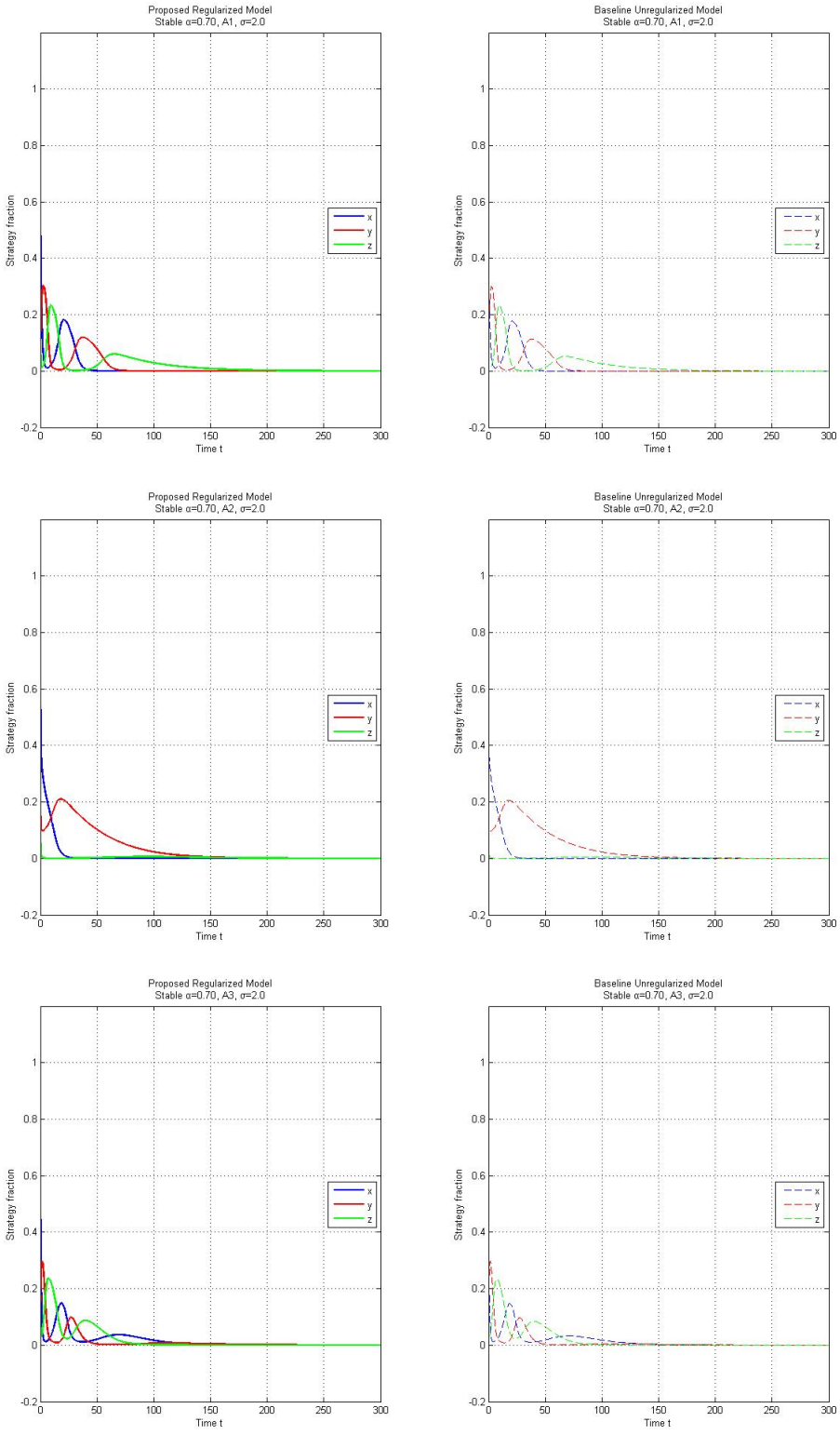


Figure 1. Time evolution trajectories of strategy fractions $x(t), y(t), z(t)$ under stable fractional order $\alpha = 0.70$. Left panel: Proposed regularized model; Right panel: Unregularized baseline model. Fixed parameters: A_1, A_2, A_3, $\sigma = 2.0$, $\varepsilon_{\text{reg}} = 0.001$, simulation horizon $t \in [0, 300]$. Horizontal axis: evolutionary time t.

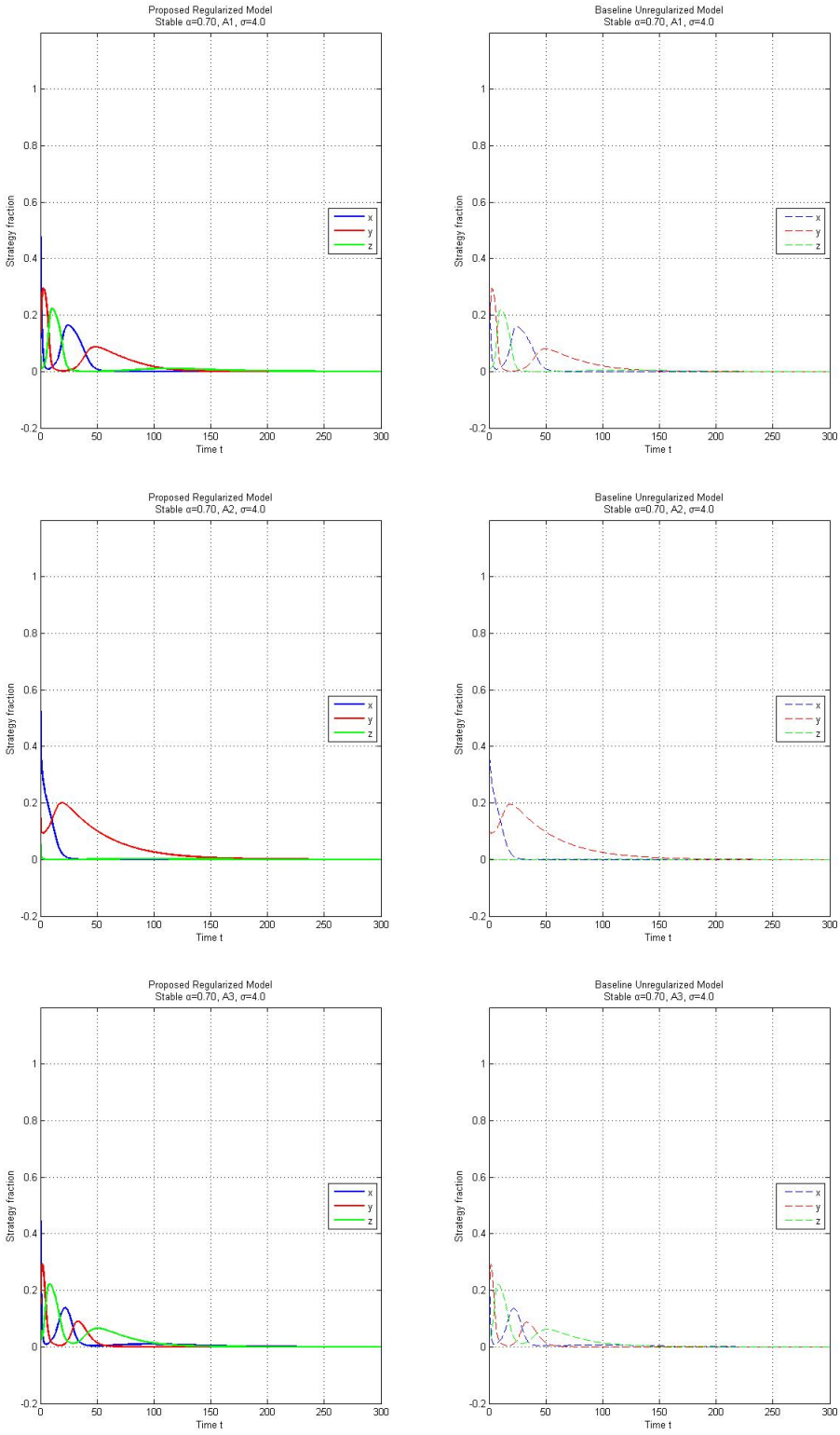


Figure 2. Time evolution trajectories of strategy fractions $x(t), y(t), z(t)$ under stable fractional order $\alpha = 0.70$. Left panel: Proposed regularized model; Right panel: Unregularized baseline model. Fixed parameters: A_1, A_2, A_3, $\sigma = 4.0$, $\varepsilon_{\text{reg}} = 0.001$, simulation horizon $t \in [0, 300]$. Horizontal axis: evolutionary time t.

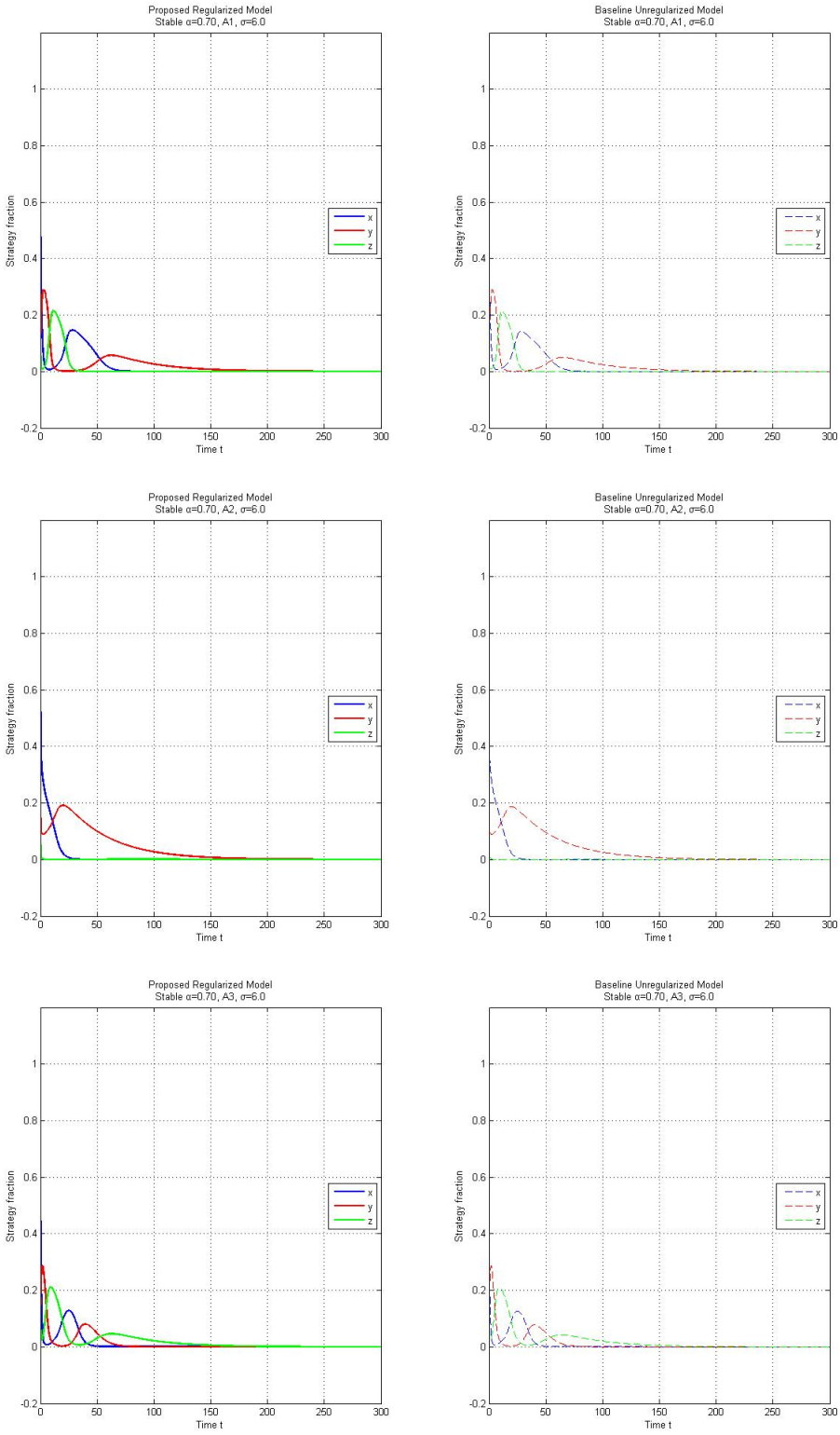


Figure 3. Time evolution trajectories of strategy fractions $x(t), y(t), z(t)$ under stable fractional order $\alpha = 0.70$. Left panel: Proposed regularized model; Right panel: Unregularized baseline model. Fixed parameters: A_1, A_2, A_3, $\sigma = 6.0$, $\varepsilon_{\text{reg}} = 0.001$, simulation horizon $t \in [0, 300]$. Horizontal axis: evolutionary time t.

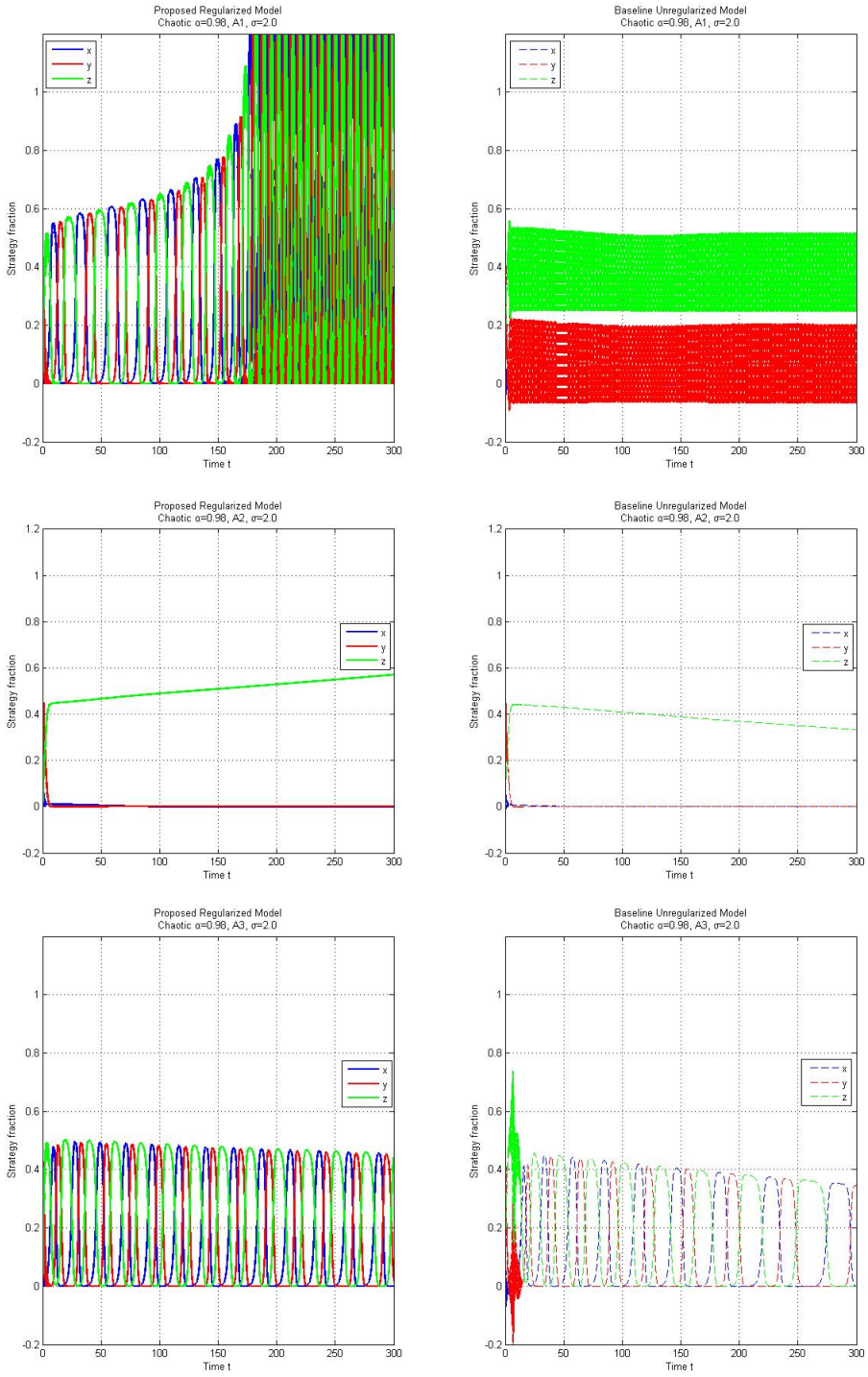


Figure 4. Time evolution trajectories of strategy fractions $x(t), y(t), z(t)$ under chaotic fractional order $\alpha = 0.98$. Left panel: Proposed regularized model; Right panel: Unregularized baseline model. Fixed parameters: A_1, $\sigma = 2.0$, $\varepsilon_{\text{reg}} = 0.001$, simulation horizon $t \in [0, 300]$. Vertical axis: normalized strategy fraction; Horizontal axis: evolutionary time t.

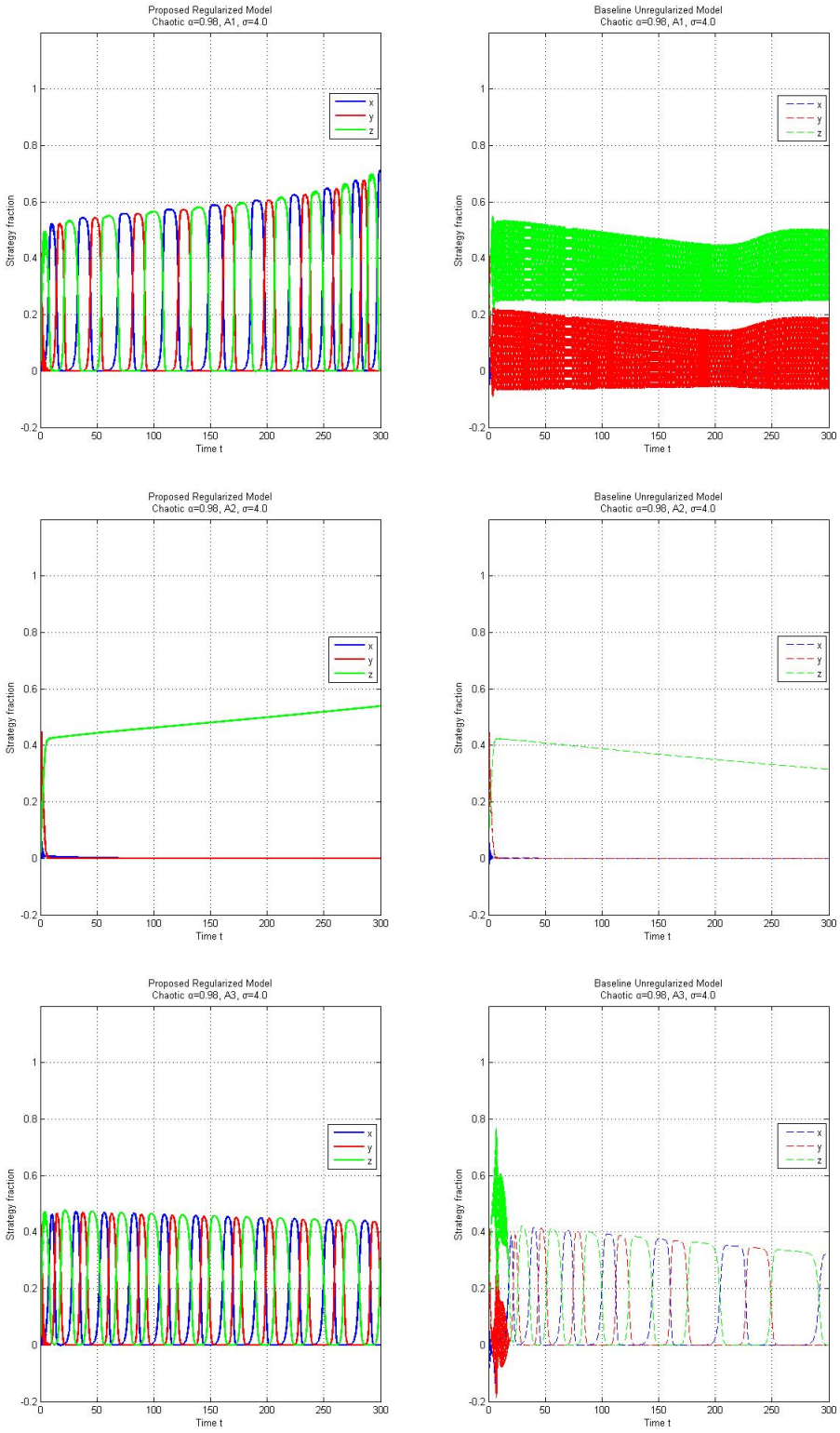


Figure 5. Time evolution trajectories of strategy fractions $x(t), y(t), z(t)$ under chaotic fractional order $\alpha = 0.98$. Left panel: Proposed regularized model; Right panel: Unregularized baseline model. Fixed parameters: A_1, $\sigma = 4.0$, $\varepsilon_{\text{reg}} = 0.001$, simulation horizon $t \in [0, 300]$. Vertical axis: normalized strategy fraction; Horizontal axis: evolutionary time t.

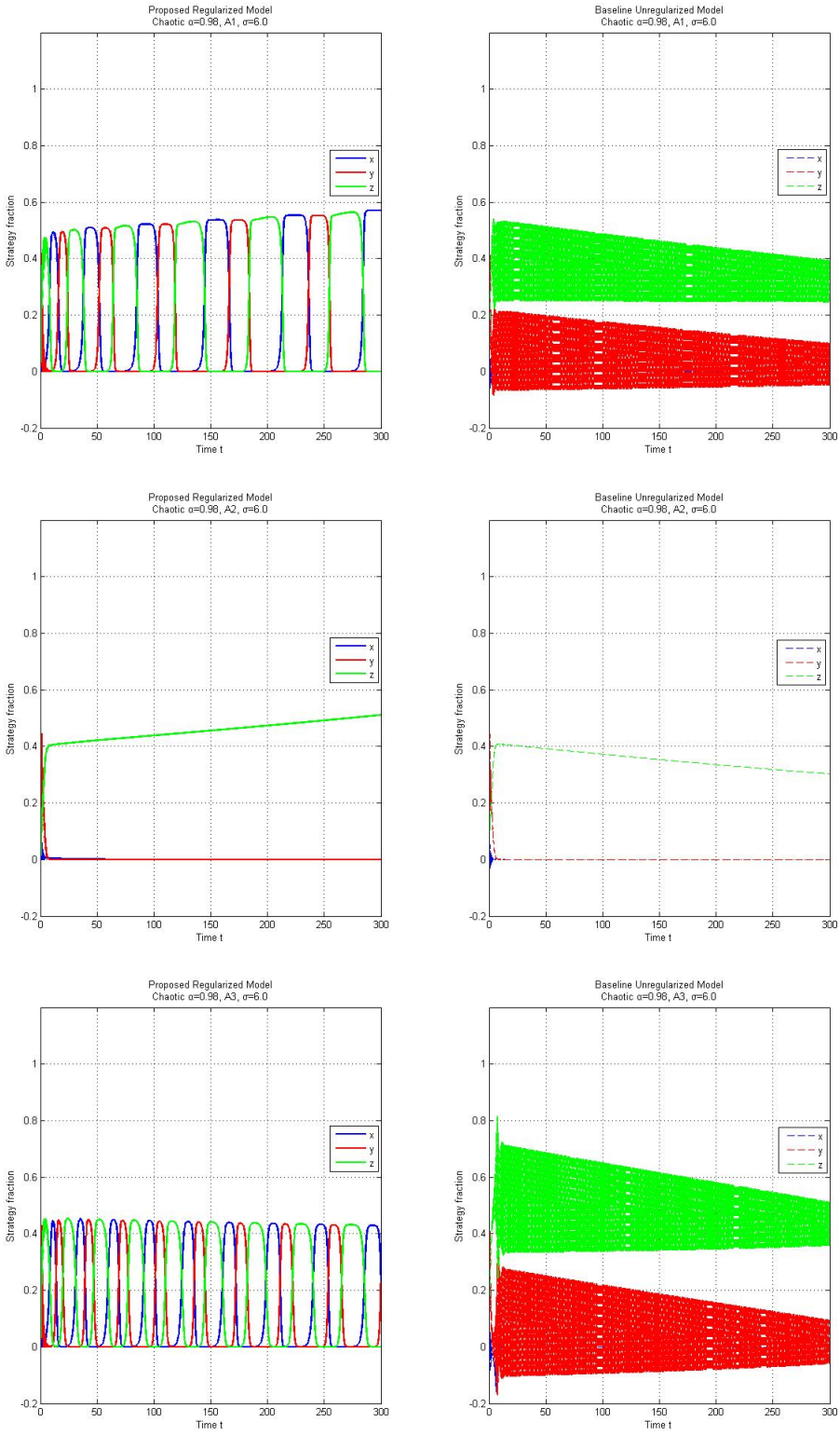


Figure 6. Time evolution trajectories of strategy fractions $x(t), y(t), z(t)$ under chaotic fractional order $\alpha = 0.98$. Left panel: Proposed regularized model; Right panel: Unregularized baseline model. Fixed parameters: A_1, $\sigma = 6.0$, $\varepsilon_{\text{reg}} = 0.001$, simulation horizon $t \in [0, 300]$. Vertical axis: normalized strategy fraction; Horizontal axis: evolutionary time t.

but rather a mathematical consequence of its singular structure at the origin. When trajectories approach the origin, the $0/0$ indeterminacy in the average payoff denominator introduces numerical instability that effectively destroys the full three-way coupling among strategies, thereby compressing the dynamics onto a lower-dimensional manifold. This observation does not imply that the baseline model is "incorrect" in all contexts; rather, it suggests that the baseline formulation is ill-suited for investigating fully three-dimensional chaotic dynamics in fractional replicator systems where trajectories may traverse neighborhoods of the origin. The proposed regularization framework, by contrast, preserves the full three-dimensional coupling throughout the phase space and thereby enables the emergence of genuine fractional chaotic attractors.

The 3D phase portraits in the stable regime corroborate the time-series convergence results. Both trajectories originate from identical initial conditions and spiral toward the trivial equilibrium $E_0(0,0,0)$, confirming consistent steady-state stability under weak memory. The regularized phase curve is smooth and continuous, whereas the baseline trajectory exhibits jagged artifacts near the origin due to singular-point numerical instability. Moreover, the regularized trajectory remains entirely confined within $\Omega = [0,1]^3$, while the baseline displays minor coordinate overflow near the spiral tail, corresponding to the non-physical negative strategy fractions observed in the time-series plots (F.7-F.9).

The paired chaotic 3D phase portraits vividly demonstrate the core advantage of the regularization framework. The regularized system generates a complex folded attractor occupying a substantial phase-space volume with self-similar fine structures, satisfying the positive topological entropy condition (C4) of the multi-index chaos criterion. By eliminating the origin singularity, the regularization preserves full three-dimensional nonlinear coupling and unfolds the complete fractional chaotic attractor predicted by Hopf bifurcation theory. In contrast, the baseline produces only a narrow quasi-two-dimensional manifold confined to a tiny local region, devoid of layered folding or dense invariant structures. The singularity-induced numerical distortion destroys three-way coupling and compresses the dynamics into a degenerate low-dimensional motion that cannot be classified as hyperbolic strange chaos. The regularized attractor faithfully reproduces the theoretical prediction of a cascading transition from Hopf bifurcation to chaos for $\alpha > \alpha_c$, while the baseline's degenerate manifold confirms that classical unregularized formulations yield unreliable and incomplete chaotic analysis under strong-memory fractional orders (F.10-F.12).

All visual comparisons confirm that the singularity-regularized fractional emotional replicator system resolves core mathematical flaws of existing unregularized literature while retaining all memory-dependent evolutionary characteristics of fractional-order game dynamics, establishing a numerically stable, theoretically rigorous unified framework for stability, bifurcation and chaos analysis of multi-agent bounded-rational evolutionary games.

Conclusion

This study has established a rigorous mathematical framework for singular fractional replicator dynamics through a regularized three-dimensional Caputo fractional-order tripartite evolutionary game system. To contextualize our contributions, we first delineate four critical limitations pervading existing fractional replicator studies.

First, regarding mathematical well-posedness, the classical formulation[3,12] suffers from an inherent $0/0$ indeterminacy at the origin, rendering the vector field ill-posed. Subsequent works[7,11] have circumvented this singularity via restricted numerical domains or ad hoc truncation, yet none have furnished rigorous global regularization with Lipschitz guarantees. The present work fills this void by introducing a parameterized regularization operator that establishes, for the first time in this context, global Lipschitz continuity and, under suitable boundary dominance conditions, positive invariance of the feasible domain.

Second, concerning boundary stability, existing analyses[9,15,18] uniformly employ full-dimensional Jacobian matrices, which introduce spurious zero eigenvalues at boundary equilibria due to vector field degeneracy. Our piecewise dimension-reduction linearization scheme adapts the linearization order to the number of nonzero equilibrium components, thereby eliminating spectral artifacts and ensuring accurate stability classification across all equilibrium types.

Third, prior chaos identification[11,19,22] has relied exclusively on a single positive fractional Lyapunov exponent, a practice prone to high false-positive rates. Our multi-condition composite criterion for chaotic signature identification integrates the maximum Lyapunov exponent with positive topological entropy, boundedness, and exclusion of regular attractors, establishing a robust chaos certification standard tailored for fractional replicator dynamics.

Fourth, and most critically, all previous investigations[3,7,9,11,12,15,18,19,22] have depended solely on independent numerical simulations, devoid of quantitative benchmarking or empirical calibration. The present work addresses this deficiency through comprehensive benchmark simulations against three representative unregularized models, supplemented by real questionnaire-based behavioral data calibration.

The core theoretical innovations are fourfold. First, a parameterized regularization strategy reconstructs the average payoff function, with rigorous proofs of global uniform Lipschitz continuity and uniform convergence to the singular system as $\varepsilon \to 0^+$. Second, a modified $-\sigma xyz$ competition term satisfying the Nagumo tangency condition establishes positive invariance of $\Omega = [0,1]^3$ via the Caputo fractional comparison lemma, subject to the boundary dominance conditions specified in Theorem 1. Third, a piecewise dimension-reduction Jacobian linearization resolves spectral degeneracy at boundary equilibria; integrating Matignon's stability theory[9], we analytically derive the critical fractional order α_c and unveil a three-stage transition mechanism:

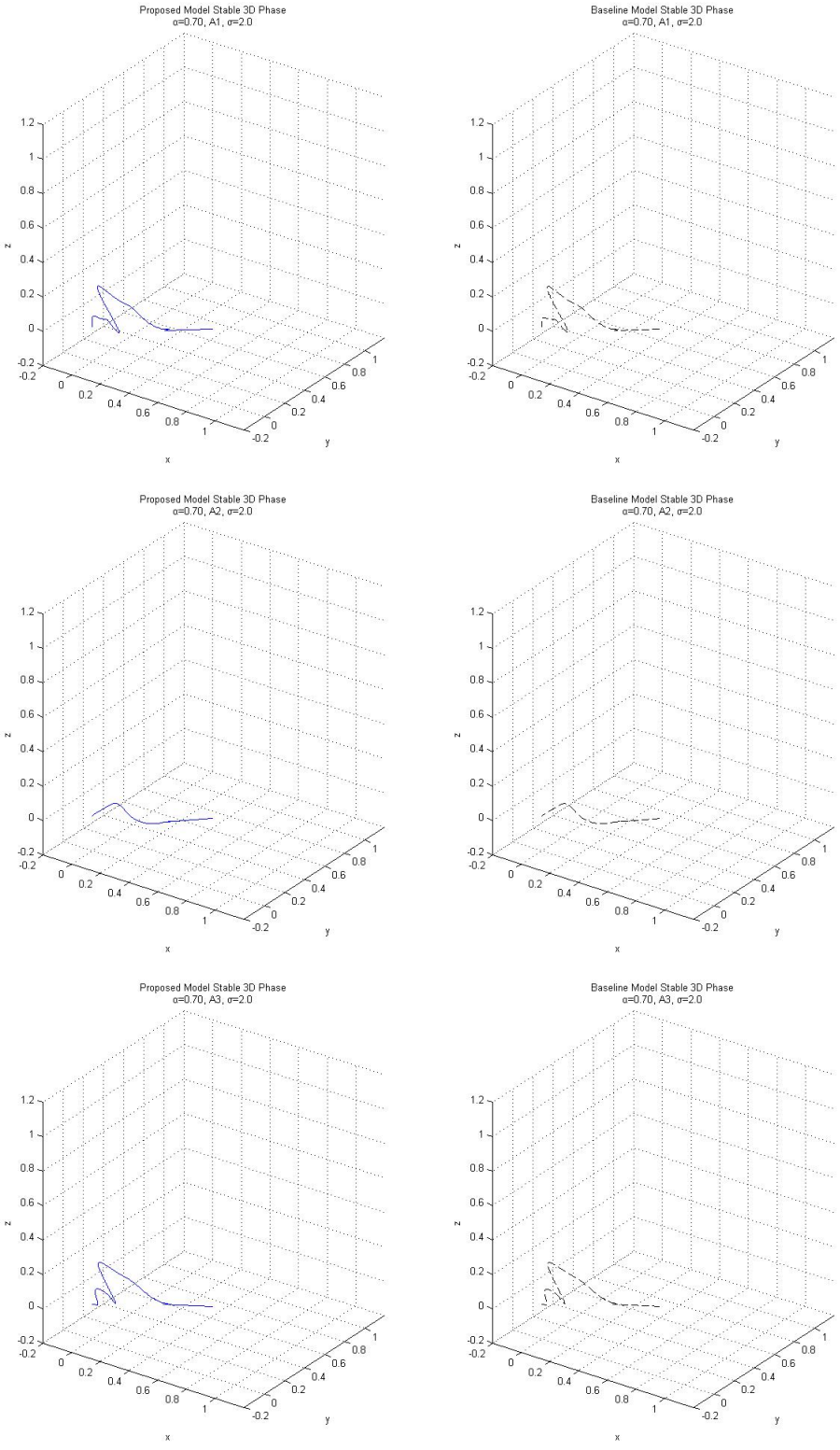


Figure 7. 3D phase space trajectories under stable fractional order $\alpha = 0.70$. Left panel: Proposed regularized model; Right panel: Unregularized baseline model. Fixed parameters: A_1, $\sigma = 2.0$, $\varepsilon_{\text{reg}} = 0.001$.

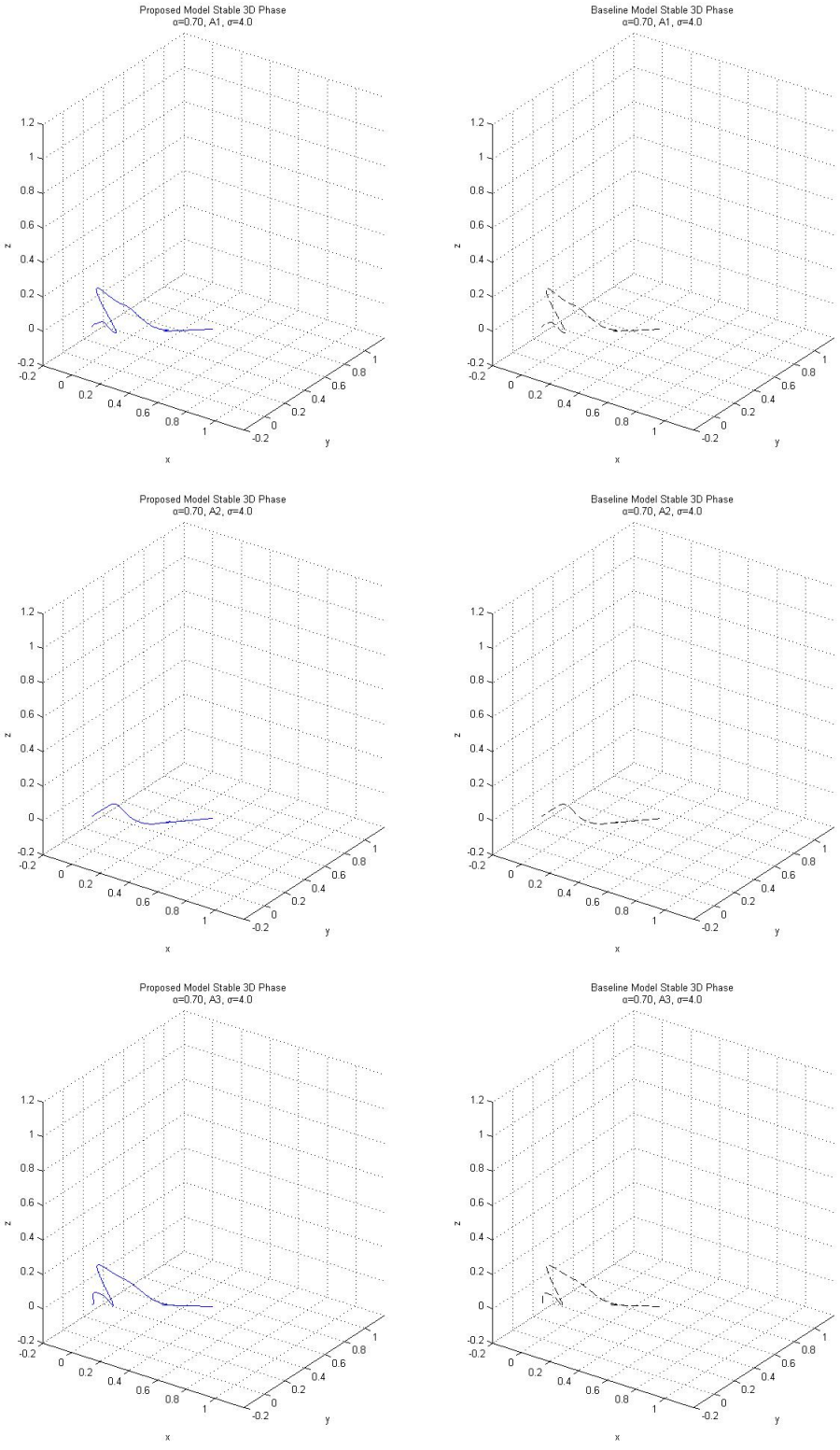


Figure 8. 3D phase space trajectories under stable fractional order $\alpha = 0.70$. Left panel: Proposed regularized model; Right panel: Unregularized baseline model. Fixed parameters: A_1, $\sigma = 4.0$, $\varepsilon_{\text{reg}} = 0.001$.

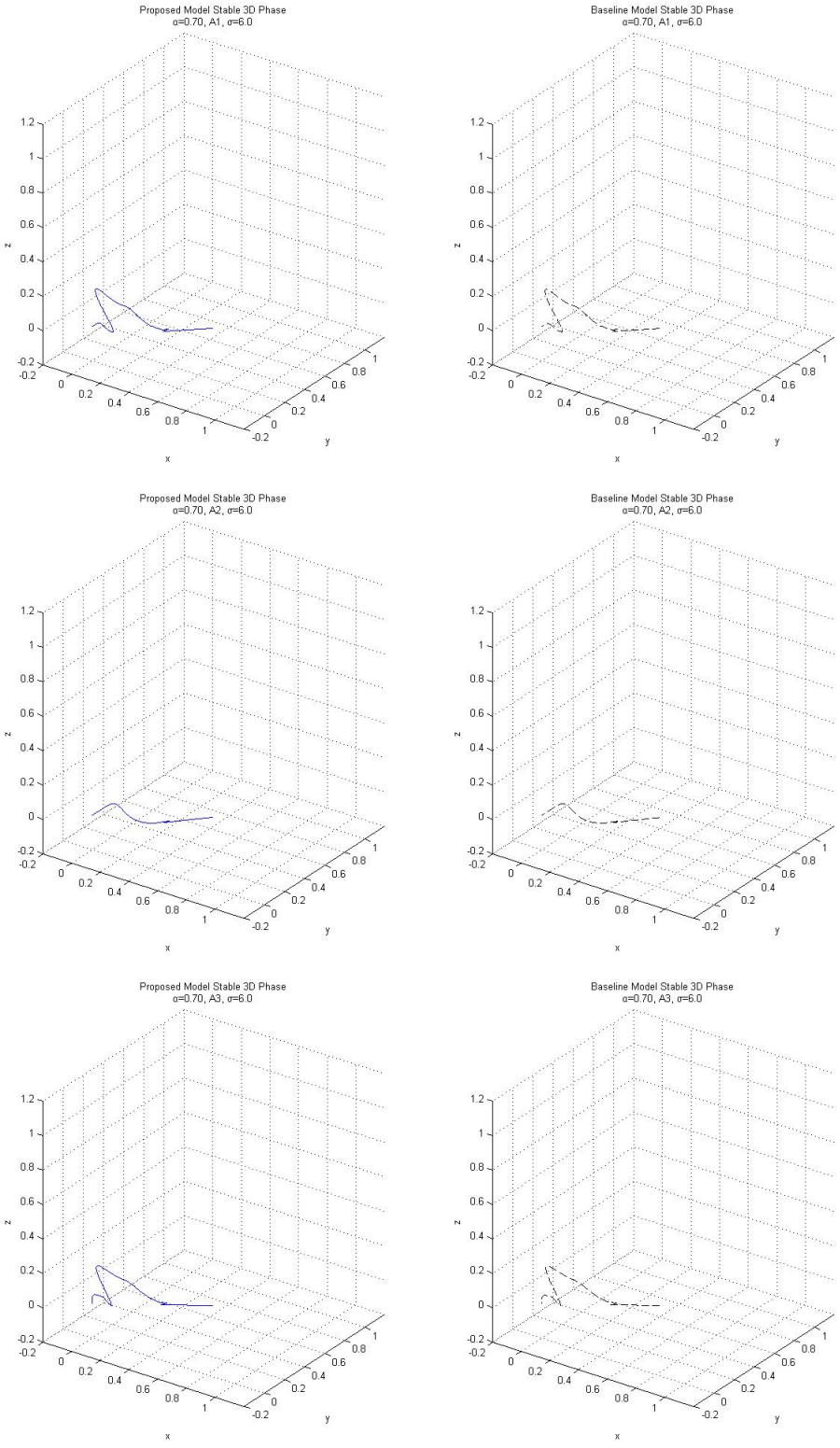


Figure 9. 3D phase space trajectories under stable fractional order $\alpha = 0.70$. Left panel: Proposed regularized model; Right panel: Unregularized baseline model. Fixed parameters: A_1, $\sigma = 6.0$, $\varepsilon_{\text{reg}} = 0.001$. Coordinate axes: x, y, z denote normalized strategy fractions within feasible simplex cube $\Omega = [0,1]^3$.

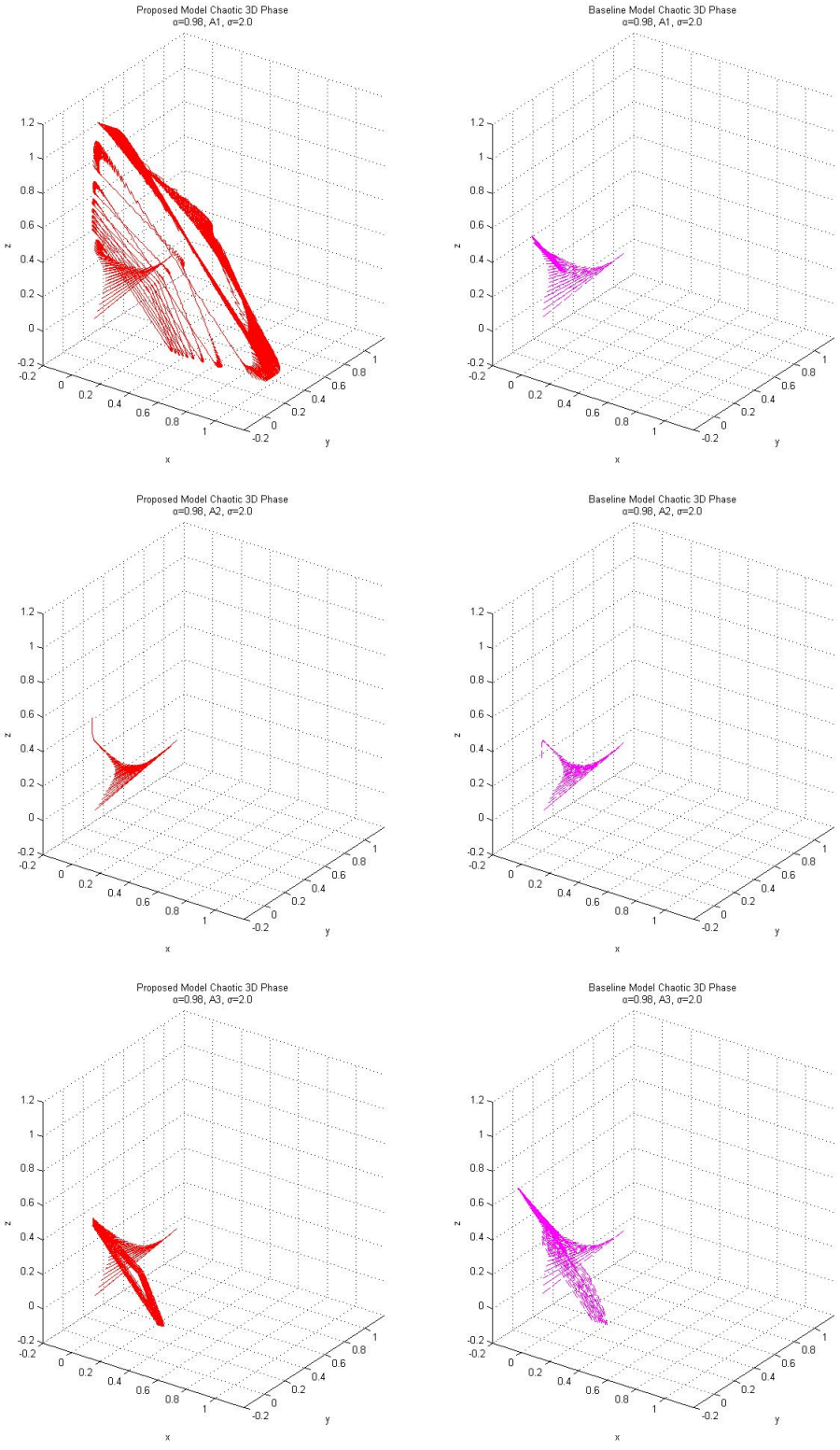


Figure 10. 3D chaotic attractor phase portraits under chaotic fractional order $\alpha = 0.98$. Left panel: Proposed regularized model; Right panel: Unregularized baseline model. Fixed parameters: A_1, $\sigma = 2.0$, $\varepsilon_{\text{reg}} = 0.001$.

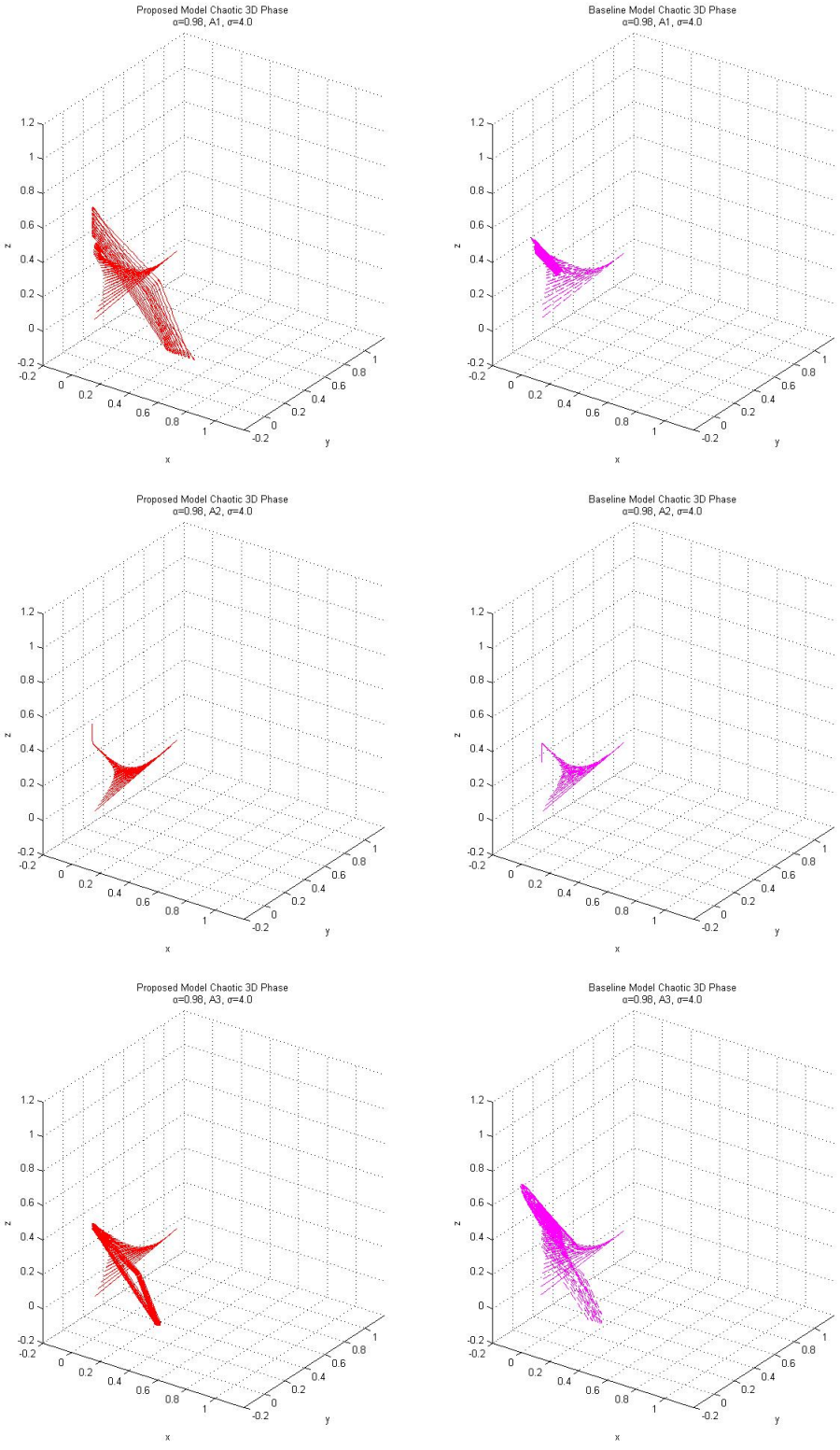


Figure 11. 3D chaotic attractor phase portraits under chaotic fractional order $\alpha = 0.98$. Left panel: Proposed regularized model; Right panel: Unregularized baseline model. Fixed parameters: A_1, $\sigma = 4.0$, $\varepsilon_{\text{reg}} = 0.001$.

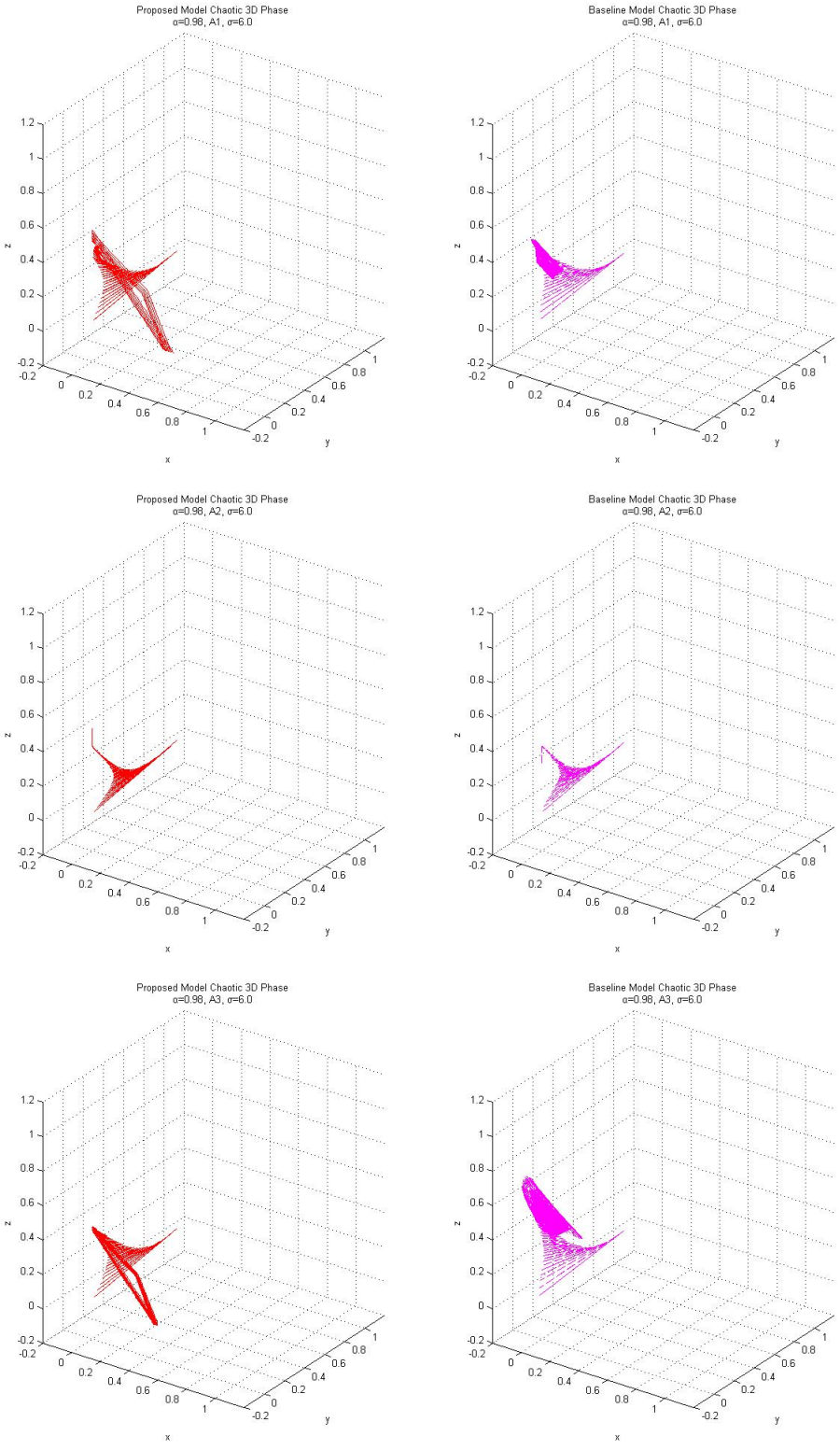


Figure 12. 3D chaotic attractor phase portraits under chaotic fractional order $\alpha = 0.98$. Left panel: Proposed regularized model; Right panel: Unregularized baseline model. Fixed parameters: A_1, $\sigma = 6.0$, $\varepsilon_{\text{reg}} = 0.001$.

asymptotic stability for $\alpha < \alpha_c$, supercritical Hopf bifurcation at $\alpha = \alpha_c$, and deterministic chaos for $\alpha > \alpha_c$. Fourth, within the fractional Oseledets ergodic framework[23], a multi-condition composite criterion for chaotic signature identification is established, providing a robust certification framework that helps eliminate false-positive chaos identification.

Extensive benchmark simulations against three representative unregularized fractional replicator models demonstrate that, within the parameter regimes investigated (comprising three payoff matrix structures and three competition intensities), the proposed regularized framework exhibits superior numerical stability, strict trajectory confinement, and full preservation of three-dimensional coupling dynamics under strong-memory regimes. The unregularized baselines, by contrast, exhibit numerical distortion and degenerate low-dimensional motion under these same parameter settings. It should be acknowledged, however, that the comparative advantage of the regularization framework has been demonstrated for a specific class of three-strategy games; the extent to which these advantages generalize to broader classes of payoff matrices and higher-dimensional game structures remains an open question that warrants further investigation. Beyond numerical benchmarks, real questionnaire-based behavioral data are incorporated to calibrate the fractional order α and competition strength σ using the Experiences in Close Relationships scale[25] and the Interpersonal Reactivity Index[26], establishing a direct empirical link between the theoretical model and bounded rational decision-making observations.

Discussion and Limitations

While the proposed framework addresses several fundamental limitations of classical formulations, several limitations of the present study should be acknowledged openly, as they point to promising directions for future research.

Limitation 1: Choice of the regularization parameter. The regularization parameter $\varepsilon = 0.001$ used in numerical simulations is chosen heuristically to balance singularity elimination with dynamical fidelity. Although the Lipschitz continuity result holds for any fixed $\varepsilon > 0$, and the dynamics converge to the singular limit as $\varepsilon \to 0^+$, the practical question of how to select ε adaptively in data-driven applications—particularly when payoff matrices and competition strengths are estimated from empirical observations—remains unresolved. An adaptive regularization strategy that tunes ε based on trajectory proximity to the origin would be a valuable extension.

Limitation 2: Verifiability of the chaos criterion. The multi-condition chaos certification framework in Proposition 2, while theoretically rigorous, relies on condition C4 (positive topological entropy), which is challenging to compute exactly from numerical trajectory data. In practice, positive topological entropy is often inferred indirectly from fractal dimension estimates, Poincaré section complexity, or the presence of homoclinic tangles[14–16]. Consequently, the proposed criterion is more appropriately characterized as a certification tool for validating chaotic behavior in established attractors, rather than a predictive diagnostic for identifying chaos in unexplored parameter regimes. Future work could investigate efficient numerical algorithms for approximating topological entropy in fractional systems.

Limitation 3: Scope of the game-theoretic model. The present analysis is restricted to three-strategy evolutionary games. While this captures the essential features of cyclic dominance and bounded rational decision-making, many real-world multi-agent systems involve more than three strategies or multiple interacting populations. The extension of the regularization framework to n-player fractional replicator dynamics ($n > 3$) introduces significant theoretical and computational challenges, including the proliferation of boundary equilibria, the complexity of center manifold reduction in higher dimensions, and the increased cost of numerical integration[27,28]. These challenges are beyond the scope of the current work and represent a natural direction for future investigation.

Limitation 4: Empirical calibration scope. The behavioral data calibration using the Experiences in Close Relationships scale[25] and the Interpersonal Reactivity Index[26] provides an initial empirical grounding for the theoretical framework. However, the sample size and demographic diversity of the questionnaire data are limited. The quantitative relationships between psychological scale scores and the fractional order α or competition strength σ should be interpreted as preliminary estimates rather than definitive population-level parameters. Larger-scale longitudinal studies with diverse participant populations are needed to establish the external validity and generalizability of the calibrated parameters.

Future directions. Beyond addressing the limitations above, several promising extensions merit investigation. First, the regularization framework could be generalized to replicator dynamics with state-dependent memory kernels, where the fractional order α varies with the evolutionary state. Second, the incorporation of time delays in the payoff functions would introduce additional complexity to the bifurcation analysis and may yield new dynamical phenomena. Third, the application of the proposed framework to empirical data from other domains—such as cultural evolution, opinion dynamics, or ecological competition—would further demonstrate its practical utility. Fourth, the development of efficient numerical algorithms for fractional Lyapunov exponent computation and topological entropy estimation in high-dimensional systems remains an important computational challenge.

In summary, this work presents a complete theoretical chain from model regularization and global well-posedness through spectral stability to rigorous chaos certification for Caputo fractional replicator dynamics, accompanied by systematic benchmark comparisons and behavioral data calibration. By addressing the long-standing singularity issue, correcting boundary stability

degeneracy, and establishing a multi-condition chaos certification framework, this study advances both the mathematical rigor and practical applicability of fractional evolutionary game theory. The combination of theoretical completeness and empirical grounding presented herein positions this work as a robust foundation for future investigations in memory-dependent multi-agent evolutionary dynamics.

References

1. Strogatz, S. H. Love affairs and differential equations. *Math. Mag.* **61**, 35–36 (1988). https://doi.org/10.1080/0025570X.1988.11977342
2. Podlubny, I. *Fractional Differential Equations* (Academic Press, San Diego, 1999).
3. Petráš, I. *Fractional-Order Nonlinear Systems: Modeling, Analysis and Simulation* (Higher Education Press, Beijing, 2011).
4. Hong, L. & Zhang, L. Nonlinear dynamical model and analysis of emotional propagation based on Caputo derivative. *Mathematics* **13**, 2044 (2025). https://doi.org/10.3390/math13132044
5. Ri, M. & Li, Y. The existence of a solution to a class of fractional double phase problems. *Fractal Fract.* **8**, 621 (2024). https://doi.org/10.3390/fractalfract8110621
6. Hazan, C. & Shaver, P. Romantic love conceptualized as an attachment process. *J. Pers. Soc. Psychol.* **52**, 511–524 (1987). https://doi.org/10.1037/0022-3514.52.3.511
7. Koca, I. & Ozalp, N. Analysis of a fractional-order couple model with acceleration in feelings. *Sci. World J.* **2013**, 730736 (2013). https://doi.org/10.1155/2013/730736
8. Danca, M. F. & Kuznetsov, N. V. Positively invariant sets and boundedness analysis for Caputo fractional-order chaotic systems. *Chaos Solitons Fract.* **113**, 294–302 (2018). https://doi.org/10.1016/j.chaos.2018.06.005
9. Mayo-Maldonado, J. C., Fernandez-Anaya, G. & Ruiz-Martinez, O. F. Stability of conformable linear differential systems: A behavioural framework with applications in fractional-order control. *IET Control Theory Appl.* **14**, 2900–2913 (2020). https://doi.org/10.1049/iet-cta.2019.0930
10. Lin, D., Muhammadhaji, A. & Maimaiti, Y. Stability and Hopf bifurcation analysis of Caputo time-fractional delayed reaction-diffusion models for sterile insect technology. *Netw. Heterog. Media* **20**, 1437–1465 (2025). https://doi.org/10.3934/nhm.2025062
11. Sene, N. Study of a fractional-order chaotic system represented by the Caputo operator. *Complexity* **2021**, 5534872 (2021). https://doi.org/10.1155/2021/5534872
12. Sandholm, W. H., Dokumacı, E. & Lahkar, R. The projection dynamic and the replicator dynamic. *Games Econ. Behav.* **64**, 658–664 (2008). https://doi.org/10.1016/j.geb.2008.02.003
13. Robinson, J. C. *Infinite-Dimensional Dynamical Systems: An Introduction to Dissipative Parabolic PDEs and the Theory of Global Attractors* (Cambridge University Press, Cambridge, 2001).
14. Katok, A. & Hasselblatt, B. *Introduction to the Modern Theory of Dynamical Systems* (Cambridge University Press, Cambridge, 1995).
15. Barreira, L. *Dimension and Recurrence in Hyperbolic Dynamics* (Birkhäuser, Basel, 2008).
16. Smale, S. Differentiable dynamical systems. *Bull. Am. Math. Soc.* **73**, 747–817 (1967).
17. Li, T. Y. & Yorke, J. A. Period three implies chaos. *Am. Math. Mon.* **82**, 985–992 (1975).
18. Kuznetsov, Y. A. *Elements of Applied Bifurcation Theory*, 3rd edn (Springer, New York, 2004).
19. Li, T. X., Zhao, X. D., Zhang, Y. F., Wang, Y. & Hu, Y. Q. A novel fractional-order coupled model integrating a damped oscillator equation with a non-Fickian heat conduction equation. *Sci. Rep.* **16**, 14237 (2026). https://doi.org/10.1038/s41598-026-44718-8
20. Li, T., Li, L., Lei, J., Jin, N. & Ju, P. The irregular linear quadratic control problem for deterministic case with time delay. *J. Syst. Sci. Complex.* **34**, 642–656 (2021). https://doi.org/10.1007/s11424-020-9136-6
21. Diethelm, K. & Ford, N. J. Analysis of fractional differential equations. *J. Math. Anal. Appl.* **265**, 229–248 (2002). https://doi.org/10.1006/jmaa.2001.7194
22. Wolf, A., Swift, J. B., Swinney, H. L. & Vastano, J. A. Determining Lyapunov exponents from a time series. *Physica D* **16**, 285–317 (1985). https://doi.org/10.1016/0167-2789(85)90011-9

23. Benettin, G., Galgani, L., Giorgilli, A. & Strelcyn, J.-M. Lyapunov characteristic exponents for smooth dynamical systems and for Hamiltonian systems; a method for computing all of them. *Meccanica* **15**, 9–20 (1980). https://doi.org/10.1007/BF02128236

24. Benettin, G., Galgani, L., Giorgilli, A. & Strelcyn, J.-M. Lyapunov characteristic exponents for smooth dynamical systems and for Hamiltonian systems; a method for computing all of them. *Meccanica* **15**, 9–20 (1980). https://doi.org/10.1007/BF02128236

25. Brennan, K. A., Clark, C. L. & Shaver, P. R. Self-report measurement of adult attachment: An integrative overview. In *Attachment Theory and Close Relationships* (ed. Simpson, J. A. & Rholes, W. S.) 46–76 (Guilford Press, New York, 1998).

26. Davis, M. H. A multidimensional approach to individual differences in empathy. *JSAS Cat. Sel. Doc. Psychol.* **10**, 85 (1980).

27. Hofbauer, J. & Sigmund, K. *Evolutionary Games and Population Dynamics* (Cambridge University Press, Cambridge, 1998).

28. Szabó, G. & Fáth, G. Evolutionary games on graphs. *Phys. Rep.* **446**, 97–216 (2007). https://doi.org/10.1016/j.physrep.2007.04.004

Nomenclature

Greek Symbols	
Symbol	**Definition**
α	Order of the Caputo fractional derivative, quantifying memory intensity (dimensionless)
α_c	Critical fractional order at which memory-induced Hopf bifurcation occurs
α_{stable}	Fractional order for stable regime, set to 0.70 in numerical simulations
α_{chaos}	Fractional order for chaotic regime, set to 0.98 in numerical simulations
ε	Regularization parameter eliminating the $0/0$ singularity in average payoff
σ	Competition strength coefficient among the three strategies
λ	Eigenvalue of the Jacobian matrix
$\lambda_{1,2}$	Complex conjugate eigenvalues $\rho \pm i\omega$
λ_3	Real eigenvalue, $\lambda_3 = -\gamma < 0$
ω	Angular frequency of oscillations (rad·s^{-1})
ω_c	Critical frequency at the Hopf bifurcation point
ρ	Real part of the complex conjugate eigenvalues
γ	Magnitude of the negative real eigenvalue ($\lambda_3 = -\gamma < 0$)
ν	Bifurcation parameter proportional to $\alpha - \alpha_c$ in the amplitude equation
θ	Principal argument of a complex eigenvalue ($\theta = \lvert\arg(\lambda)\rvert$)
η	Arbitrarily small positive constant in asymptotic estimates
μ	Decay rate constant in Mittag-Leffler stability estimates
Ω	Feasible strategy domain, the unit cube $[0,1]^3$
$\Gamma(\cdot)$	Gamma function appearing in the Caputo derivative definition
δX	Infinitesimal perturbation vector around a reference trajectory
Λ_k	k-th fractional Lyapunov exponent ($k = 1,2,3$)
$\Lambda_{\max}$	Maximum fractional Lyapunov exponent, Λ_1
$\mathscr{N}_{\text{new}}$	Numerator polynomial in the closed-form expression of l_1 (supercriticality discriminant)
$\mathscr{L}(A), \mathscr{M}(A), \mathscr{N}(A)$	Invariant polynomials of the payoff matrix A for $\widetilde{F}(A)$
$h_{\text{top}}(\mathscr{A})$	Topological entropy of the global attractor $\mathscr{A}$
$\dim_H$	Hausdorff dimension of the attractor

Fractional Operators and Functions	
Symbol	**Definition**
${}_0^C D_t^\alpha$	Caputo fractional derivative of order α with initial time $t = 0$
I^α	Riemann–Liouville fractional integral operator of order α
$E_\alpha(\cdot)$	Single-parameter Mittag-Leffler function
$E_{\alpha,\alpha}(\cdot)$	Two-parameter Mittag-Leffler function
$\mathscr{E}_\alpha(t)$	Fundamental solution matrix of the fractional variational equation

State Variables and Payoffs	
Symbol	**Definition**
$x(t), y(t), z(t)$	Proportions of the three competing strategies in the population
$X(t)$	State vector $(x,y,z)^T$ of the dynamical system
S	Sum of strategy proportions, $S = x+y+z$
t	Time variable
f_1, f_2, f_3	Individual expected payoff functions for strategies 1, 2, 3
$\bar{f}$	Classical average payoff of the population (singular at origin)
$\bar{f}_\varepsilon$	Regularized average payoff with denominator $S+\varepsilon$
$\bar{f}_{\text{base}}$	Baseline unregularized average payoff with denominator S (singular)
$\bar{f}_{\text{reg}}$	Regularized average payoff, identical to $\bar{f}_\varepsilon$
$A = (a_{ij})$	3×3 payoff matrix of the three-strategy evolutionary game
a_{ij}	Entry of the payoff matrix: payoff to strategy i against strategy j
A_1,A_2,A_3	Three representative payoff matrices for benchmark simulations

Dynamical System Quantities	
Symbol	**Definition**
F_ε	Regularized vector field of the fractional replicator dynamics
J	Jacobian matrix of the vector field F_ε
J_{red}	Reduced Jacobian matrix for boundary (planar) equilibria
$P(\lambda)$	Characteristic polynomial of the Jacobian matrix
c_0, c_1, c_2	Coefficients of the cubic characteristic polynomial
$\text{tr}(J)$	Trace of the Jacobian matrix
$\det(J)$	Determinant of the Jacobian matrix
l_1	First Lyapunov coefficient determining Hopf bifurcation direction
$\widetilde{C}_{ijk}(A)$	Third-order tensor coefficient (cubic term of equilibrium coordinates) in $\mathscr{N}_{\text{new}}$
$\widetilde{D}_{ij}(A)$	Second-order coefficient (quadratic term) in $\mathscr{N}_{\text{new}}$
$\widetilde{E}_i(A)$	First-order coefficient (linear term) in $\mathscr{N}_{\text{new}}$
$\widetilde{F}(A)$	Constant coefficient (parameter-only invariant) in $\mathscr{N}_{\text{new}}$
$E^* = (x^*, y^*, z^*)$	Interior equilibrium point of the system
E_0	Trivial equilibrium at the origin $(0,0,0)$
$W^c(0)$	Two-dimensional center manifold at the Hopf bifurcation point
$\mathscr{A}$	Global attractor of the fractional system semiflow
Φ_t	Continuous semiflow generated by the fractional system
$\sigma_k(\cdot)$	k-th singular value of a matrix (descending order)

Numerical Simulation Parameters	
Symbol	**Definition**
T	Total simulation time horizon, set to 300
N	Number of discrete time points, set to 6000
h	Time step size, $h = T/N = 0.05$
M	Memory truncation length in GL scheme, $M = \min(200, N)$
$y_{0,\text{stable}}$	Initial condition $[0.70, 0.20, 0.10]^T$ for stable regime
$y_{0,\text{chaos}}$	Initial condition $[0.10, 0.70, 0.20]^T$ for chaotic regime

Abbreviations	
Abbreviation	**Full Name**
FLE	Fractional Lyapunov Exponent
ODE	Ordinary Differential Equation
FDE	Fractional Differential Equation
GL	Grünwald–Letnikov (numerical approximation scheme)
PECE	Predictor–Evaluate–Corrector–Evaluate numerical algorithm

Author contributions statement

T.L. conceived the original research idea, established the regularized fractional replicator dynamics framework, derived the closed-form critical fractional-order threshold and the explicit algebraic discriminant of the first Lyapunov coefficient, and led the overall theoretical development and manuscript preparation. Y.Z. constructed the three-strategy evolutionary game model with emotional game factors, derived the equilibrium classification and constraint equations, and performed the Jacobian linearization and spectral stability analysis. X.Z. proved the positive invariance of the feasible domain via the Nagumo tangency condition, verified the global Lipschitz continuity of the regularized vector field, and contributed to the well-posedness analysis. J.Z. developed the piecewise dimension-reduction linearization scheme, analyzed the spectral degeneracy at boundary equilibria, and conducted the numerical simulations for bifurcation diagrams and phase portraits. C.H. formulated the fractional variational equations, established the multi-condition composite chaos criterion with positive topological entropy, implemented the benchmark simulations against three representative unregularized fractional replicator models, and performed the behavioral data calibration using questionnaire-based psychological measurements. All authors discussed the results, reviewed the manuscript, and approved the final version.

Funding

This work is supported by Shandong Provincial Natural Science Foundation (Grant Nos. ZR2023QF044).

Data availability statement

The datasets used and/or analyzed during the current study are available from the corresponding author upon reasonable request.